THE JOURNAL OF PHYSICAL CHEMISTRY C

KoBSON

Subscriber access provided by KoBSON

C: Plasmonics; Optical, Magnetic, and Hybrid Materials

Combined Experimental and Theoretical Investigation of the Origin of Magnetic Anisotropy in Pentagonal Bipyramidal Isothiocyanato Co(II), Ni(II) and Fe(III) Complexes With Quaternary Ammonium-functionalized 2,6-Diacetylpyridine Bisacylhydrazone

Darinka Darmanovi#, Igor Nikolaevic Shcherbakov, Carole Duboc, Vojislav Spasojevi#, Darko Hanzel, Katarina An#elkovi#, Dušanka Radanovi#, Iztok Turel, Milica Milenkovi#, Maja Gruden, Božidar #obelji#, and Matija Zlatar

J. Phys. Chem. C, **Just Accepted Manuscript** • DOI: 10.1021/acs.jpcc.9b08066 • Publication Date (Web): 26 Nov 2019

Downloaded from pubs.acs.org on December 2, 2019

Just Accepted

"Just Accepted" manuscripts have been peer-reviewed and accepted for publication. They are posted online prior to technical editing, formatting for publication and author proofing. The American Chemical Society provides "Just Accepted" as a service to the research community to expedite the dissemination of scientific material as soon as possible after acceptance. "Just Accepted" manuscripts appear in full in PDF format accompanied by an HTML abstract. "Just Accepted" manuscripts have been fully peer reviewed, but should not be considered the official version of record. They are citable by the Digital Object Identifier (DOI®). "Just Accepted" is an optional service offered to authors. Therefore, the "Just Accepted" Web site may not include all articles that will be published in the journal. After a manuscript is technically edited and formatted, it will be removed from the "Just Accepted" Web site and published as an ASAP article. Note that technical editing may introduce minor changes to the manuscript text and/or graphics which could affect content, and all legal disclaimers and ethical guidelines that apply to the journal pertain. ACS cannot be held responsible for errors or consequences arising from the use of information contained in these "Just Accepted" manuscripts.

is published by the American Chemical Society. 1155 Sixteenth Street N.W., Washington, DC 20036

Published by American Chemical Society. Copyright © American Chemical Society. However, no copyright claim is made to original U.S. Government works, or works produced by employees of any Commonwealth realm Crown government in the course of their duties.

Combined Experimental and Theoretical Investigation of the Origin of Magnetic Anisotropy in Pentagonal Bipyramidal Isothiocyanato Co(II), Ni(II) and Fe(III) Complexes With Quaternary Ammonium-functionalized 2,6-diacetylpyridine Bisacylhydrazone

Darinka Darmanović[†], Igor N. Shcherbakov[‡], Carole Duboc[§], Vojislav Spasojević[||], Darko Hanžel[⊥], Katarina Anđelković[†], Dušanka Radanović[#], Iztok Turel[▽], Milica Milenković[†], Maja Gruden[†], Božidar Čobeljić[†] and Matija Zlatar*[#]*

[†]Faculty of Chemistry, University of Belgrade, Studentski trg 12-16, 11000 Belgrade, Serbia

[‡]Faculty of Chemistry, Southern Federal University, Zorge 7, 344090, Rostov-on-Don, Russia

[§]Département de Chimie Moléculaire, University Grenoble Alpes/CNRS, 38000 Grenoble, France

[‖]Institute of Nuclear Sciences 'Vinča', Condensed Matter Physics Laboratory, P.O. Box 522, 11001 Belgrade, Serbia

[⊥]Jozef Stefan Institute, Jamova 39, SI-1000 Ljubljana, Slovenia

[#]Department of Chemistry, Institute of Chemistry, Technology and Metallurgy, National Institute, University of Belgrade, Njegoševa 12, 11000 Belgrade, Serbia.

[▽]Faculty of Chemistry and Chemical Technology, University of Ljubljana, Večna pot 113, 1000, Ljubljana, Slovenia

ABSTRACT: The magnetic anisotropy in pentagonal bipyramidal complexes of Co(II) (**1** and **2**), Fe(III) (**3** and **4**) and Ni(II) (**5**) with 2,2′-[2,6-pyridinediylbis(ethylidyne-1-hydrazinyl-2-ylidene)]bis[*N*,*N*,*N*-trimethyl-2-oxoethanaminium] equatorial ligand and isothiocyanato axial ligands has been investigated by magnetic susceptibility measurements, powder X-band EPR spectroscopy, Mössbauer spectroscopy, *ab initio,* and LFDFT calculations. The studied complexes display three distinct types of magnetic anisotropy. Co(II) complexes (**1** and **2**) show an easy plane anisotropy with large and positive *D* values and negligible rhombicity. Ni(II) complex (**5**) has uniaxial magnetic anisotropy with negative *D* value. Fe(III) complexes (**3** and **4**) have small ZFS parameters. Theoretical modeling was used to rationalize the magnetic anisotropy in these systems and to identify the most important excited states that are responsible for the zero-field splitting. These excitations are a consequence of the electronic structure of the central metal ion in ideal pentagonal bipyramidal coordination.

1. INTRODUCTION

Single-molecule magnets (SMMs) are paramagnetic molecular metal complexes that can retain their magnetization after removal of the magnetic field below a certain temperature.[1–4] Due to their magnetic bistability and slow magnetic relaxation, that originates from double-well potential with the magnetization reversal barrier U_{eff}, SMMs have attracted considerable attention for their potential applications in ultrahigh-density information storage and quantum computing.[5–9] Technological applications of SMMs are limited by very low blocking temperature T_B for the reversal of magnetization. The height of the magnetization reversal barrier U_{eff} depends on the total spin of the system (S) and is proportional to the product $|D|\cdot S^2$ for integer spins and $|D|\cdot(S^2\text{-}1/4)$ for half-integer spins (D is the axial zero-field splitting (ZFS) parameter).[10,11] An earlier approach to obtain larger U_{eff} and higher T_B for molecular magnets have been mainly focused on increasing the total ground spin of the molecule by the synthesis of large polynuclear complexes. In the past decade, the high magnetic anisotropy, characterized by the ZFS parameter D, is considered to be the most important for high-performance SMMs.[4,12,13] It was shown that D is inversely proportional to S^2 value,[12,13] making an increase in the spin ground state not effective way to increase U_{eff}. Magnetic anisotropy is the dependence of magnetic properties on the spatial directions of an applied magnetic field.[14] The spin direction may be flipped (in the relaxation process) due to the thermal crossing of the energy barrier, or tunneling effects usually quantified by rhombic ZFS parameter E.[10,15] Magnetic anisotropy is influenced by multiple factors such as coordination number, molecular symmetry, ligand-field strength, spin-orbit coupling (SOC). Therefore, design, control and fine-tuning of the magnetic anisotropy is a challenging task.[13–22] It is noteworthy to mention that magnetic anisotropy is very sensitive to the surrounding of a central metal ion and is therefore also employed to explore the oxidation states, spin states and coordination modes of transition metal complexes.[23]

Examples of systems with very large magnetic anisotropy are complexes of transition metals in linear geometry.[24–26] However, large magnetic anisotropy is not limited to low-coordination numbers,[14] but also to other coordination geometries where the d-orbital splitting pattern is similar to the linear geometry, e.g., trigonal bipyramidal[19] or pentagonal bipyramidal geometry (PBPY-7), Figure 1.

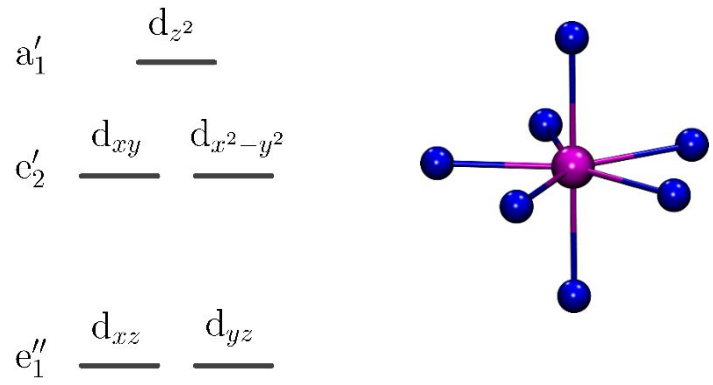

Figure 1 Qualitative orbital splitting diagram for pentagonal bipyramidal (PBPY-7) coordination (D_{5h} symmetry)

PBPY-7 Co(II) complexes are relatively common and show magnetic anisotropy with D values in the range of 13-68 cm^{-1}.[27–46] On the other hand, Ni(II) complexes in PBPY-7 environment are scarce.[47] The rare examples of PBPY-7 Ni(II) complexes, with magnetic properties investigated, involve mononuclear high-spin Ni(II) complexes[32,33,35,40,43,46] as well as two pentanuclear $[Ni_3W_2]$ compounds containing the PBPY-7 Ni(II) moieties associated with $[W(CN)_8]^{3-}$.[48]

Bis(acylhydrazones) of 2,6-diacetylpyridine are suitable ligands for the synthesis of metal complexes with PBPY-7 coordination polyhedron. The chelating diversity of these types of ligands is influenced by their flexibility in assuming different conformations, the possibility of coordination in neutral, mono- and doubly deprotonated forms and high coordination capacity.[49] In the complexes, hydrazone pentadentate ligand is coordinated in an equatorial plane through the pyridine nitrogen atom, two azomethine nitrogen atoms and two carbonyl

oxygen atoms forming four fused five-membered metal-chelate rings, while the rest two axial coordination places are occupied with monodentate ligands.[50]

Recently, our group synthesized and structurally characterized PBPY-7 isothiocyanato Co(II), Ni(II) and Fe(III) complexes with 2,2′-[2,6-pyridinediylbis(ethylidyne-1-hydrazinyl-2-ylidene)]bis[*N*,*N*,*N*-trimethyl-2-oxoethanaminium] ligand (Scheme 1).[51,52] In this work, we investigated the magnetic anisotropy of these complexes using magnetic measurements, EPR spectroscopy, Mössbauer spectroscopy, and theoretical calculations. Theoretical modeling was used to confirm the experimental determination of the ZFS parameters and to rationalize the magnetic anisotropy in these complexes.

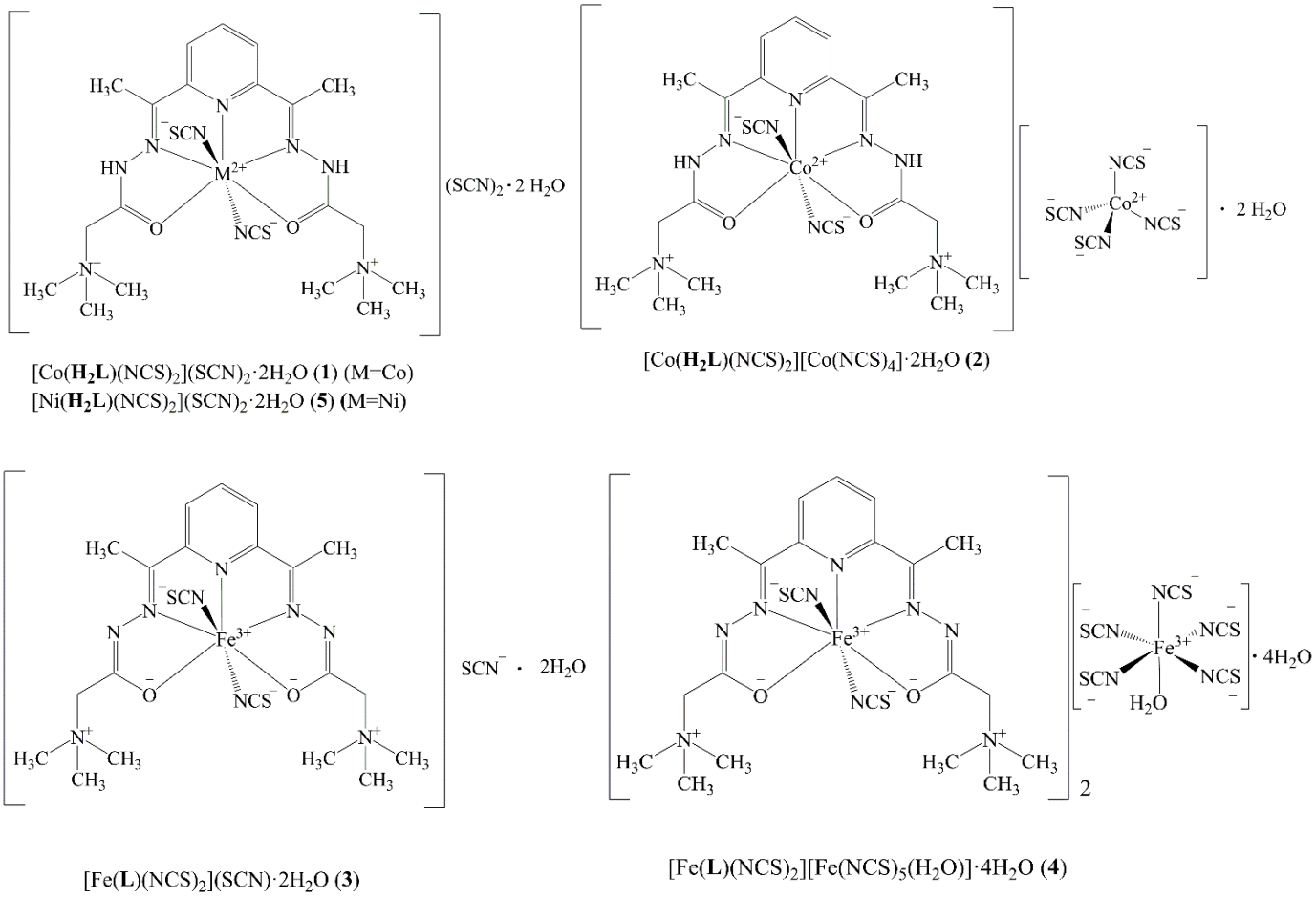

Scheme 1 Structures of pentagonal-bipyramidal isothiocyanato complexes of Co(II) (**1** and **2**), Fe(III) (**3** and **4**), Ni(II) (**5**) with 2,2′-[2,6-pyridinediylbis(ethylidyne-1-hydrazinyl-2-ylidene)]bis[*N*,*N*,*N*-trimethyl-2-oxoethanaminium] ligand (**L**).

2. EXPERIMENTAL

2.1 Synthesis

Pentagonal-bipyramidal isothiocyanato complexes of Co(II) (**1** and **2**), Fe(III) (**3** and **4**) and Ni(II) (**5**) with 2,2′-[2,6-pyridinediylbis(ethylidyne-1-hydrazinyl-2-ylidene)]bis[N,N,N-trimethyl-2-oxoethanaminium] ligand were synthesized using previously described methods.[51,52]

2.1 Magnetic Measurements

The temperature dependence of magnetic susceptibility was measured on the powder sample in the temperature range T = 2–300K, in the magnetic field of 1000 Oe, by employing a commercial Quantum Design MPMS-XL-5 SQUID magnetometer. For complexes **1** and **2** additional M(*H*) measurement were performed in the magnetic fields up to 5 T and at T = 2, 5, 10 and 15 K. The experimental data for all samples (**1**–**5**) were corrected for the contributions of the sample holder and the diamagnetism calculated from Pascal's constants. Magnetic properties have been analyzed by using the Curie-Weiss law from where Curie constants *C* and Curie-Weiss temperatures θ are determined. Standard spin Hamiltonian was used to calculate magnetic susceptibility χ_{calc}, ZFS parameters and to fit experimental data, Eq. (1):

$$H = -2\sum_{i<j}^{i,j\in N} J_{ij}S_iS_j + g\mu_B S\cdot H + D\left[S_{z^2} - \frac{S(S+1)}{3}\right] + E(S_{x^2} - S_{y^2}) \quad (1)$$

In order to account for the contribution of intermolecular exchange interaction, mean-field approximation was applied,[1] Eq. (2), from where molar susceptibility χ_M was obtained:

$$\chi_M = \frac{\chi_{calc}}{1 - \frac{zJ}{N_A\mu_B^2}\chi_{calc}} \quad (2)$$

The first term in the Eq. (1) is the exchange interaction between paramagnetic centers, the second is the Zeeman splitting, while the last two describe axial and rhombic crystal field splitting with ZFS parameters *D* and *E*, respectively. *J* was calculated only for complexes **(2)** and **(4)** with two and three complex ions in an asymmetric unit (Scheme 1). Spin-Hamiltonian was solved using the PHI software package,[53] from where χ_{calc} was obtained. The contribution of possible intermolecular exchange interactions was taken into account with Eq. (2).[53]

2.3 EPR Spectroscopy

Powder X-band EPR spectra were recorded with a Bruker EMX, equipped with an ER-4192 ST Bruker cavity and an ER-4131 VT combined with an Oxford Instruments ESR-900 continuous-flow helium cryostat for low-temperature experiments. The spectra were simulated by using the EasySpin program supported by Matlab.[54]

2.4 Mössbauer Spectroscopy

Transmission Mössbauer spectra were recorded on powder samples using a constant acceleration Wissel spectrometer and Oxford Instruments continuous flow cryostat in the temperature range between 4.2 and 295K. A 10mCi ^{57}Co radioactive source in rhodium matrix has been used, and isomer shifts are reported relative to the centroid of a spectrum of thin alpha-Fe foil at 295K. Spectra were analyzed using the least-squares fitting program.

2.3 Computational Methods

Two approaches were used for calculations of the magnetic anisotropy parameters. The first one is the post-Hartree-Fock multi-reference wavefunction approach based on the state averaged complete active space self-consistent field calculations (SA-CASSCF),[55–57] followed by the N-electron valence second-order perturbation theory (NEVPT2)[58–61] with ORCA v. 4.0 program.[62,63] Scalar relativistic effects were taken into account by a standard second-order Douglas-Kroll-Hess (DKH) procedure.[64] A segmented all-electron relativistically contracted

version[65] of Ahlrichs polarized triple-ζ basis set def2-TZVP[66–68] was used for all atoms. The resolution of identity approximation with corresponding correlation fitting of the basis set[69] was employed. The ZFS parameters, based on the dominant spin-orbit coupling contributions from excited states, were calculated through quasi-degenerate perturbation theory (QDPT),[70] in which the effective Hamiltonian theory[71] was utilized. The CASSCF active space was constructed from five MOs with predominant contribution of 3d-AOs of the metal center and n electrons, corresponding to metal ion electronic d-shell configuration (CAS(n, 5), n = 5, 7 and 8, correspondingly for Fe(III), Co(II) and Ni(II) compounds). All possible multiplet states arising from the d^n configuration were included into wavefunction expansion. For Co(II) compound 10 quartet and 40 doublet states were accounted, for Ni(II) - 10 triplet and 15 singlet states. For Fe(III) 1 sextet and 24 quartet states were calculated, while 75 doublet states arising from d^5 configuration were neglected. Splitting of the d-orbitals was analyzed within the *ab initio* ligand field theory (AI-LFT),[72,73] as implemented in ORCA software.

The second method used for the calculation of the ZFS parameters is the Ligand-field DFT (LFDFT) approach by C. Daul et al.[74,75] LFDFT procedure works by evaluating the DFT energy of all the microstates arising from the d^n configuration (252 Slater determinants for the case of d^5, 120 for the case of d^7 and 45 for the case of d^8 configuration) of the transition-metal ion surrounded with coordinating ligands, using Kohn−Sham (KS) orbitals. The KS orbitals are generated in an average of configuration (AOC) spin-restricted calculation with all d electrons distributed evenly over the five KS MOs dominated by d orbitals (Figures S6-S8 in SI). Calculations were carried out with Amsterdam Density Functional (ADF) code[76–78] at OPBE[79] level of theory with a TZP basis set and scalar relativistic Zero Order Regular Approximation (ZORA).[80,81] This set of energies is then analyzed within a ligand-field model to determine the parameters of inter-electronic repulsion (Racah parameters B and C) and one-electron 5×5 LF matrix, in a least-square sense. These parameters are used to obtain variationally the energy

and multideterminant wave function of the ground and excited states. Spin-orbit coupling constant was deduced from the least square fit of the energy splitting of the spinors, obtained by the ZORA spin-orbit DFT calculations, to the one-electron ligand field model. The ZFS parameters were deduced using an effective Hamiltonian approach[71] from the lowest eigenvalues and corresponding eigenvectors from LF-DFT multiplet calculations in the basis of ±1/2 and ±3/2 (for Co(II)), ±1/2, ±3/2, ±5/2 for (Fe(III)) and 0, ±1 (for Ni(II)) M_s wavefunctions.

All the calculations were performed on the complex ions from experimentally determined X-ray structures of **1** (CCDC 1429633),[51] **2** (CCDC 1429634),[51] **3** (CCDC 1543583)[52], **4** (CCDC 1543584)[52] and **5 (**CCDC 1429635).[51] In the case of **(2)**, calculations have been performed on both PBPY-7 cation and on $[Co(NCS)_4]^{2-}$ anion. In the case of **4**, two independent heptacoordinated Fe(III) complex cations and $[Fe(NCS)_5(H_2O)]^{2-}$ complex anion were considered. Positions of hydrogen atoms were optimized employing DFT with B3LYP hybrid functional[82] and Ahlrichs polarized basis set def2-TZVP, while positions of all other nuclei were fixed.

3. RESULTS AND DISCUSSION

3.1 Magnetic measurements

Magnetic measurements revealed that for complex **1** (Figure 2a), χ*T value at 300K is 2.5 emuK/molOe, higher than the theoretical spin-only value of 1.875 emuK/molOe for single Co(II) ion with S = 3/2 and g = 2. This phenomenon is typical for Co(II) ion due to the orbital contribution.[83,84] Upon cooling from 300 K to 50 K, χ*T decreases gradually and then significantly faster, reaching minimum value of 1.54 emuK/molOe at 2 K. This decrease at lower temperatures is a consequence of depopulation of excited Co(II) levels which arise after splitting of ground states mainly due to the crystal field and spin-orbit coupling.[84] Also, the

highest value of magnetization data at 2 K and 5 T were found to be 2.25 μ_B (Figure 2a inset), which is lower than the theoretical value of 3.0 μ_B expected for Co(II) ion, speaking in favor of large magnetic anisotropy in this system. Fitting χ^{-1}(T) experimental data to the Curie–Weiss law in the range of 50–300K, the magnetic moment of 4.57 μ_B and Curie-Weiss temperature θ = –5.4K were found. This magnetic moment is in accordance with values of 4.5–5.2 μ_B found for Co(II) ion.[83] Negative value of Curie-Weiss constant indicates the possible existence of weak antiferromagnetic interactions among molecules. During the calculation employed by using PHI software package,[53] χ*T and M(H) data for all temperatures were fitted simultaneously. Perfect match with D = 30.01 cm^{-1}, E =0.00 cm^{-1}, g = 2.32, zJ = – 0.03 cm^{-1} was achieved. This result is in agreement with Co(II) in similar PBPY-7 geometry with the pentadentate equatorial ligands.[27–35,39–46]

Complex **2** contains two Co(II) ions, with one of them having the same PBPY-7 geometry as in previously described complex **1**, while the other is in tetrahedral (T-4) coordination. Due to magnetic anisotropy, the experimentally found χ*T value of 5.35 emuK/molOe (Figure 2b) is higher than theoretical spin-only value of 3.75 emuK/molOe, expected for two Co(II) ions with S = 3/2 and g=2 at 300 K. Simultaneous fitting of experimental M(H) and χ*T data was performed assuming possible exchange interactions between two paramagnetic Co(II) within the monomer unit. Since these two ions are differently coordinated, two corresponding sets of fitting parameters from Eq. (1) were determined simultaneously. The best fit for PBPY-7 coordination gives D_1 = 36.56 cm^{-1}, E_1= 0.95 cm^{-1}, g_1 = 2.35, while parameters for tetrahedral site are D_2 = –3.90 cm^{-1}, E_2 = 0.28 cm^{-1} and g_2 = 2.17 (full lines in Figure 1b). The obtained D for $[Co(NCS)_4]^{2-}$ is in accordance with previously reported $|D|$=3.80 cm^{-1}.[85] Very small antiferromagnetic exchange interaction of J= –0.02 cm^{-1} between two paramagnetic Co(II) centers is obtained. This interaction is achieved through the very weak intramolecular hydrogen

bonds of C-H---S type (C--S distances: 3.482 and 3.817 Å) with the Co(PBPY-7)---Co(T-4) separation of 8.276 Å.[51]

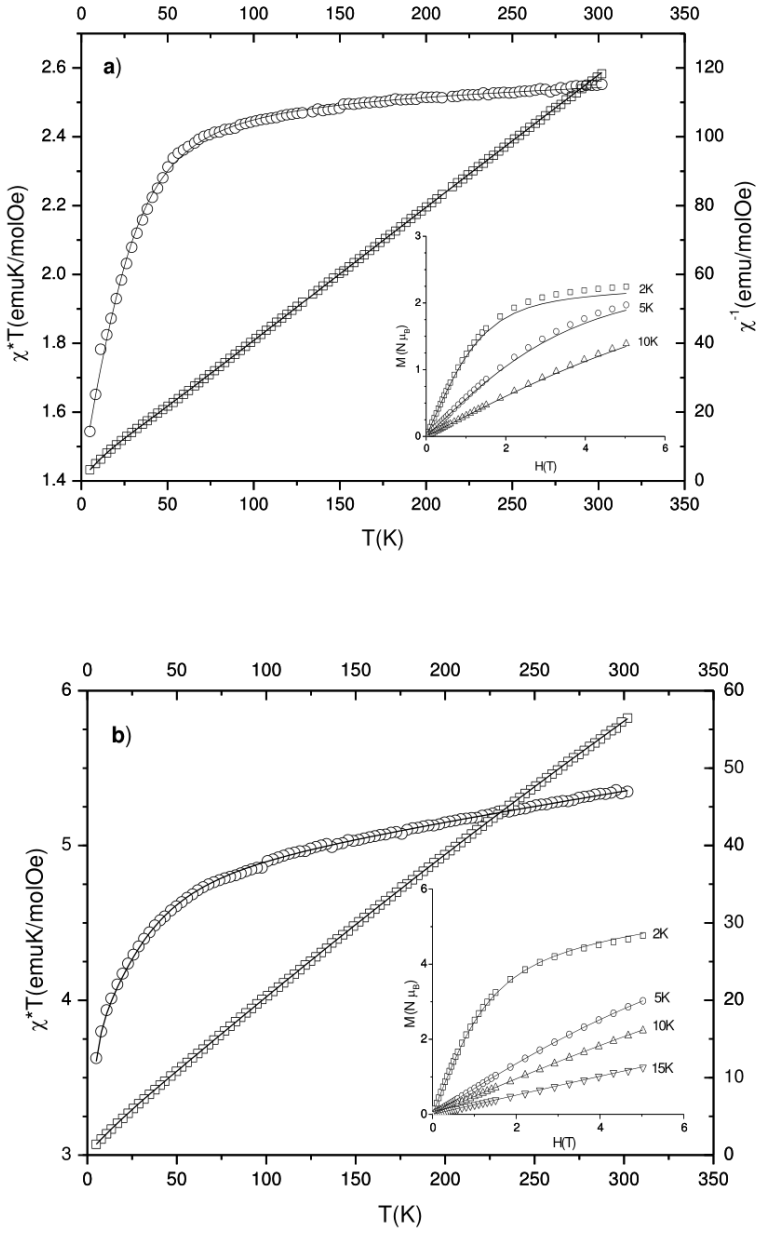

Figure 2 Experimental χ*T, M(H) and χ^{-1}(T) data (open symbols): a) for **1** and b) for **2**. Full lines represent the best fits calculated with spin Hamiltonian in Eq. (2) with parameters: D = 30.01 cm^{-1}, E = 0.00 cm^{-1}, g = 2.32, zJ = –0.03 cm^{-1} for **1**; D_1 = 36.56 cm^{-1}, E_1= 0.95 cm^{-1}, g_1 = 2.35 (PBPY-7 site), D_2 = -3.90 cm^{-1}, E_2 = 0.28 cm^{-1} and g_2 = 2.17 (T-4 site) and zJ=0.00 for **2**.

Magnetic behavior of the complex **3** is shown in Figure 3a, in the form of χ*T and χ^{-1} vs. T. At room temperature χ*T = 4.58 emuK/molOe is almost constant up to 50 K and at the lower temperatures decreases reaching minimum of 4.06 emuK/molOe at 2 K. χ*T value at 300 K is close to expected theoretical value 4.375 emuK/molOe for single Fe(III) ion with five unpaired electrons and g = 2. This agreement between χ*T values suggests that for this complex very small magnetic anisotropy should be expected. Fitting to Eq. (2) with the minimal set of parameters gave very good matching with experimental data (Figure 3a full lines). Small values of ZFS parameters D = 1.57 cm^{-1}, E=0.12 cm^{-1} confirm the assumption that the system shows a small anisotropy.

Complex **4** contains three Fe(III) ions, of which two are heptacoordinated, while the third one is in the octahedral (OC-6) environment. From the Figure 3b it is visible that χ(T)*T behavior is very similar to the previous case, indicating very weak exchange interactions among three Fe(III) ions, i.e., the almost cumulative effect of paramagnetic ions can be observed. For temperatures above 50K, χ*T display constant value of 12.77 emuK/molOe, which is close to 13.12 emuK/molOe, expected for three Fe(III) ions with S = 5/2, g = 2 at 300 K. Assuming that two ions in PBPY-7 geometry have the same fitting parameters, following values of parameters are extracted: $D_1 = D_2 = -0.50$ cm^{-1}, $E_1 = E_2 = -0.01$ cm^{-1}, $g_1 = g_2 = 1.99$ for seven-coordinated and D_3 = 0.23 cm^{-1}, E_3 = –0.01 cm^{-1} and g_3 = 2.011 for octahedral geometry. Weak antiferromagnetic interactions among three Fe(III) ions are obtained: between two ions in PBPY-7 geometry $J_{PBPY7\text{-}PBPY7}$= –0.02 cm^{-1} and between hepta- and octacoordinated ions $J_{PBPY7\text{-}OC6}$= –0,03 cm^{-1}. Structural analysis of this complex has shown that possible exchange path between two heptacoordinated sites is through intramolecular CH--π-chelate ring (Fe-N-N-C-O) interactions (C-chelate ring separation 2.900 Å).[52] Coupling between octa- and hepta-coordinated Fe(III) ions is possible through almost linear intramolecular hydrogen bond between aqua ligand and amide nitrogen (O_{water} -N_{amide} distance is 2.788 Å).[52] This favors

the weak antiferromagnetic interactions that have also been found in some three-nuclear iron(III) complexes.[86]

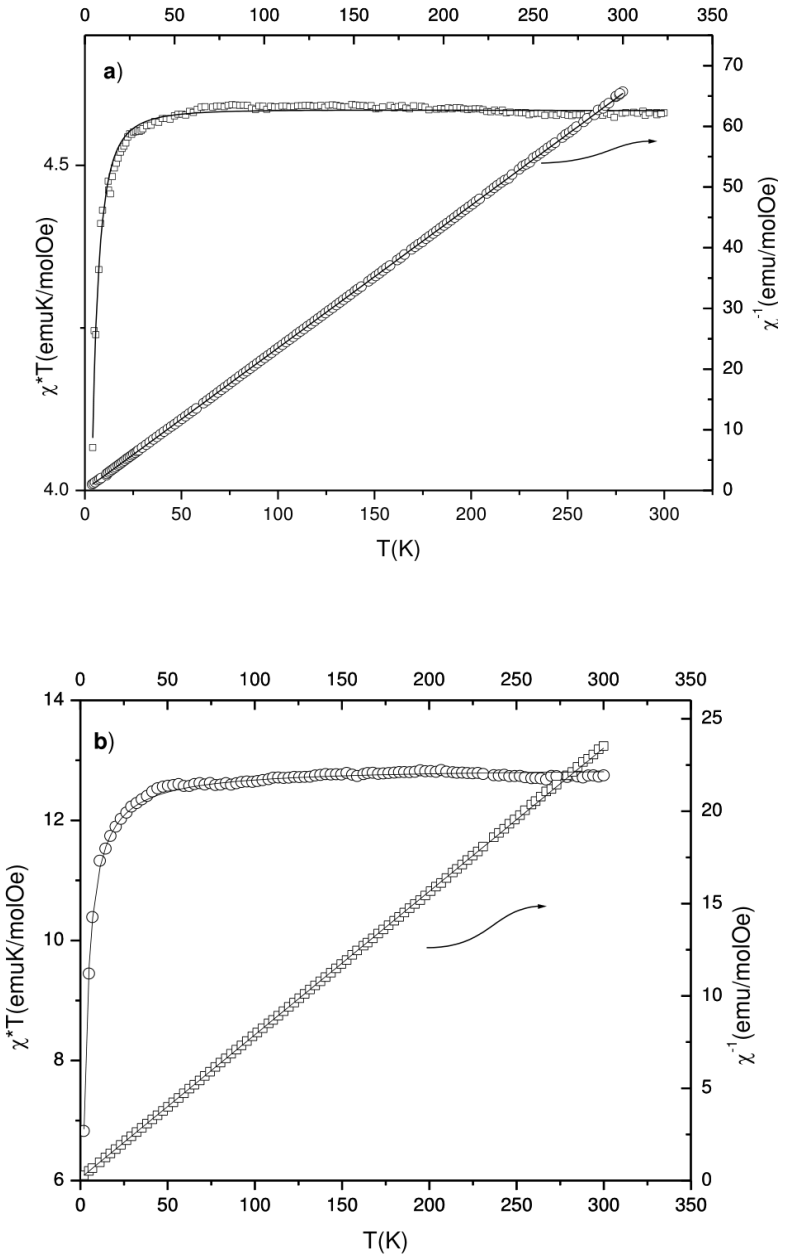

Figure 3 Experimental χ*T, M(H) and χ^{-1}(T) data (open symbols): a) for **3** and b) for **4**. Full lines represent the best fits calculated with parameters: D = 1.57 cm^{-1}, E = 0.12 cm^{-1}, g = 2.0, *zJ=0.01* for **3**; $J_{PBPY7\text{-}PBPY7}$ = –0.02 cm^{-1}, $J_{PBPY7\text{-}OC6}$ = –0,03 cm^{-1}, $D_1 = D_2$ = –0.50 cm^{-1}, $E_1 = E_2$ = –0.01 cm^{-1}, $g_1 = g_2$ = 1.99 (PBPY-7 site) and D_3 = 0.23 cm^{-1}, E_3 = 0.01 cm^{-1}, g_3 = 2.01 (OC-6 site) and zJ = –0.01 cm^{-1}for **4**

Magnetic behavior of seven-coordinated Ni(II) complex **5** is depicted in Figure 4. Experimentally found χ*T value of 1.42 emuK/molOe is much higher than theoretically expected value 1.00 emuK/molOe for S = 1, g = 2.0 at 300 K, due to high magnetic anisotropy. A similar higher χ*T value of 1.3 emuK/molOe was found for similar Ni(II) complexes with PBPY-7 geometry,[40] showing that, like in Co(II) cases, this coordination causes high magnetic anisotropy. Spin Hamiltonian was fitted to the experimental data and results are depicted in Figure 4 as full lines, with $D = -11.71$ cm^{-1}, $E = -1.48$ cm^{-1}, $g = 2.31$, $zJ = -0.04$ cm^{-1}.

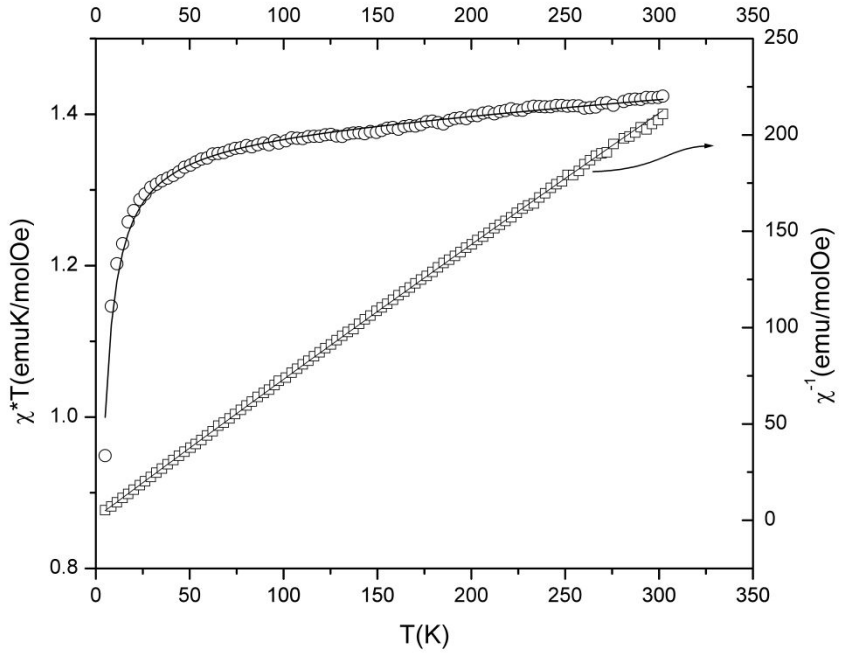

Figure 4 Experimental χ*T, M(H) and χ^{-1}(T) data (open symbols) for **5.** Full lines represent the best fits with parameters: $D = -11.71$ cm^{-1}, $E = -1.48$ cm^{-1}, $g = 2.31$, $zJ = -0.04$ cm^{-1}

3.2 EPR Spectroscopy

Complex **1** displays nice powder EPR spectra at low temperatures up to 50 K, Figure 5a. The spectrum is dominated by a resonance located at the low field with respect to $g = 2.00$ (~330 mT), at 164 mT, in agreement with a high spin Co(II) ion $S = 3/2$. The featureless aspect of this signal is consistent with an axial system ($E/D \sim 0$). The absence of resonances at the higher field is consistent with a large D magnitude, much larger than the energy provided by the X-band EPR spectrometer ($|D| \gg 0.3$ cm^{-1}). In such low field conditions, the shape of the EPR spectrum is not dependent on the D value, but only on the E/D ratio. Simulation of the experimental spectrum based on Eq (1), Figure 5a, confirms that E/D is close to zero (E/D = 0.03) in agreement with the parameters determined from the magnetization experiments.

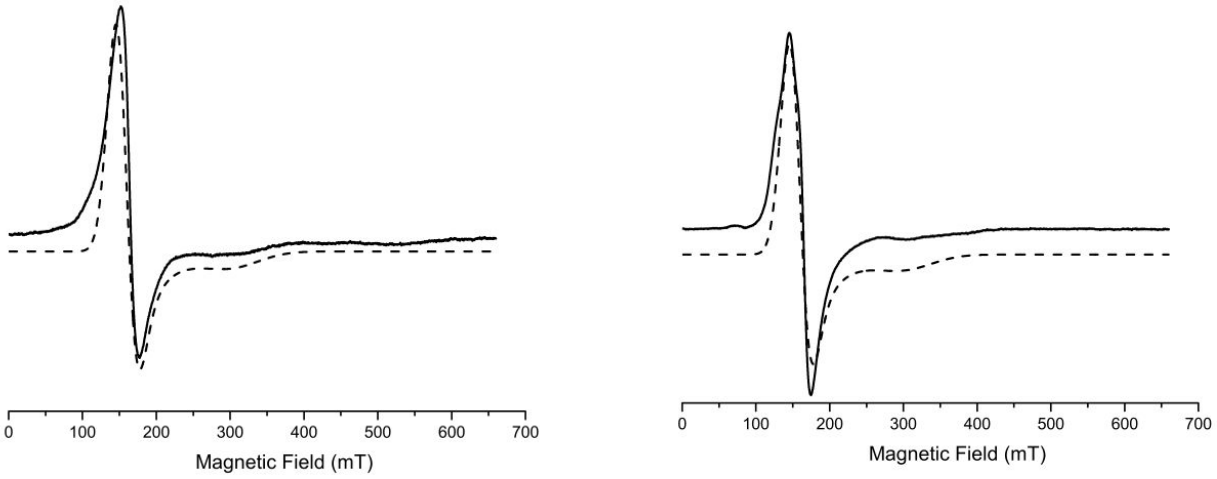

a) b)

Figure 5 Experimental (solid line) and simulated (dashed line) powder EPR spectra of a) complex **1** (15 K). Parameters used for the simulation: $E/D = 0.03$, $g = 2.17$ (a large D magnitude was taken arbitrary $|D| = 30$ cm^{-1}). b) complex **2** (10 K). Parameters used for the simulation: Co(II) ion (site with the PBPY-7 geometry) $|D| = 30$ cm^{-1}, $E/D = 0.02$, g = 2.22; Co(II) ion (tetrahedral site) $|D| = 4.50$ cm^{-1}, $|E| = 0.47$ cm^{-1}, $E/D = 0.10$, $g = 2.33$

In complex **2**, the presence of two Co(II) sites complicates the powder X-band EPR spectra recorded below 50 K. Interestingly, the well-defined features of both sites can be observed. As an example, the spectrum recorded at 10 K is shown in Figure 5b. The resonance observed at ~170 mT, corresponding to the Co site with the PBPY-7 geometry is similar to that in the spectrum of complex **1**. Figure S1 in the SI highlights the difference between the spectra of **1** and **2**, especially in the shape of the feature located at low field. Consequently, additional features can be assigned to the second site. They also correspond to a high spin Co(II) (S = 3/2), with two features at low field and one at 301 mT. The shape of this spectrum is consistent with a smaller *D* magnitude with spectra sensitive to both ZFS parameters. By taking into account a 1:1 ratio for the Co(II) sites, the ZFS parameters for this second site can be precisely determined using Eq. (1), with $|D|$ = 4.5 cm-1, $|E|$ = 0.47 cm-1, E/D = 0.10, g = 2.33. Only an isotropic *g*-value was applied for the simulation process to avoid overparameterization. The quality of the simulated spectrum combined with the magnetization data makes us confident in the determined ZFS parameters.

The two Fe(III) complexes display similar powder X-band EPR spectra (Figures 6a and 6b) with features only between 0 and 500 mT, consequently with high spin Fe(III) complex (S = 5/2). The simulation of the spectrum of complex **3** (Figure 6a) that contains only one Fe(III) site in an heptacoordinated environment provides ZFS parameters that well agree with the magnetization data: $|D|$ = 1.67 cm^{-1}, $|E|$ = 0.17 cm^{-1}, E/D = 0.10, g = 2.05. The spectrum of complex **4** (Figure 6b) is less resolved due to the presence of two Fe(III) sites with comparable ZFS parameters. By taking into account a 2:1 ratio (corresponding to population of 7-:6-coordination sites) between the two Fe(III) sites during the simulation process, we found that the heptacoordinated Fe(III) site displays ZFS parameters similar to that of complex **3**: $|D|$ = 1.57 cm^{-1}, $|E|$ = 0.16 cm^{-1}, E/D = 0.10, g = 1.98. The decrease in the *D* magnitude is observed

through both EPR and magnetization experiments. This can be rationalized by modifications due to different packing of the complexes. The second Fe(III) site located in an octahedral environment is characterized by: $|D| = 2.17$ cm^{-1}, $|E| = 0.17$ cm^{-1}, $E/D = 0.08$, g = 1.95.

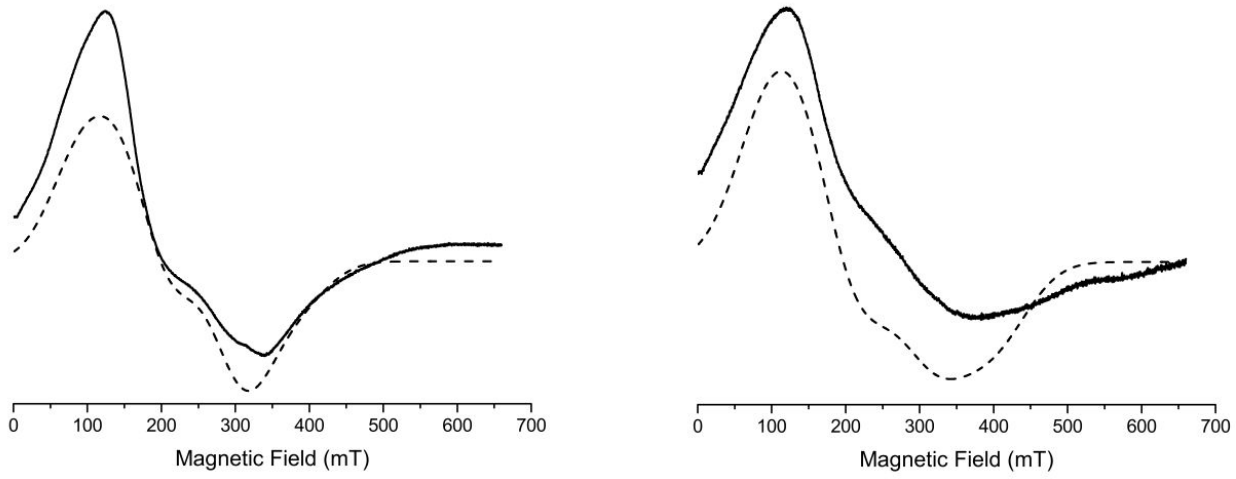

a) b)

Figure 6 Experimental (solid line) and simulated (dashed line) powder EPR spectra of a) complex **3** (15 K). Parameters used for the simulation: $|D| = 1.67$ cm^{-1}, $|E| = 0.17$ cm^{-1}, $E/D = 0.10$, $g = 2.05$. b) complex **4** (18 K). Parameters used for the simulation: Fe(III) ion (site in a heptacoordinated environment) $|D| = 1.57$ cm^{-1}, $|E| = 0.16$ cm^{-1}, $E/D = 0.10$, $g = 1.98$; Fe(III) ion (octahedral site) $|D| = 2.17$ cm^{-1}, $|E| = 0.17$ cm^{-1}, $E/D = 0.08$, $g = 1.95$.

Complex **5** displays powder EPR spectra at low temperatures (in the range 5-30 K). For integer spin state only systems with low to moderate ZFS values can be observed at X-band frequency. Because only two transitions are observed in the low field part of the spectra (Figure 7) at around ~140 mT and ~170 mT, a moderate D magnitude is expected (range 0.33- 6.50 cm^{-1}). Simulation confirms this analysis: $|D| = 0.56$ cm^{-1}, $|E| = 0.18$ cm^{-1}, $E/D = 0.32$, g = 2.13. This D magnitude is much lower than that determined by magnetization. Besides, since larger D-magnitudes are expected for PBPY-7 geometry (in the range ca. -7 to -17 cm^{-1}),[32,33,35,40,43,46]

we conclude that the observed spectrum arises from the presence of impurities in the powder. The *ab initio* predicted ZFS-values for complex **5** confirms this hypothesis (see below).

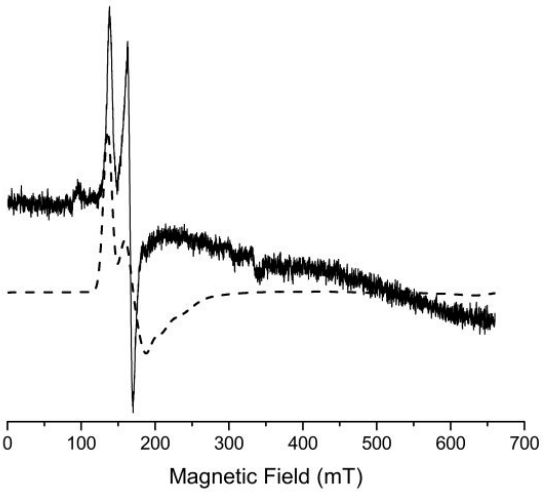

Figure 7 Experimental (solid line) and simulated (dashed line) powder EPR spectra (15 K) of complex **5**. Parameters used for the simulation: $|D| = 0.56$ cm^{-1}, $|E| = 0.18$ cm^{-1}, $E/D = 0.32$, $g = 2.13$.

3.3 Mössbauer spectroscopy

^{57}Fe Mössbauer spectra were recorded in the temperature range between 4.2K and 295K without applied magnetic field (Figure 8), to confirm the oxidation and spin state of the Fe centers in **3** and **4**. Room temperature spectra of **3** and **4** are very similar (Figures S2-S5 in SI, for a comparison of overlaid spectra of **3** and **4** recorded at 295K), however the tri-nuclear spectrum belonging to **4** showed some structure around minimum of the spectrum, while the spectrum belonging to **3** resembled a shape of a broad singlet. Spectra of **3** and **4** recorded at 4.2K did not show any magnetic ordering, however, the isomer shifts were increased compared to spectra recorded at room temperature and the spectra were broadened, which can be seen on the shoulders of spectra. All spectra of **3** and **4** have been fitted by using a dynamic lineshape site analysis,[87] assuming that the magnetic field is flipping parallel to the z-direction of axially

symmetric electric field gradient (η=0). Hyperfine magnetic fields were fixed to an arbitrary value of 30T because the relaxation times and magnetic field are correlated and cannot be fitted independently. Isomer shifts at 295K for heptacoordinated Fe(III) in **3** and **4** were 0.445 and 0.54 mm/s, respectively, while in the octahedral coordinated Fe(III) site was 0.41 mm/s, which are typical values for high-spin Fe(III). The spectral area ratio between hepta- and octahedral coordinated Fe(III) in **4** was within error margins identical to the theoretical one of 2:1. The calculated dwell times between flips were 1.25×10^{-9}s and 3.12×10^{-9} s for **3** at 295K and 4.2K, respectively, and for octahedral coordination of Fe(III) in **4** 3.2×10^{-10}s and 9.36×10^{-10}s at 295K and 4.2K, respectively, and for heptacoordinated Fe(III) in **4** 1.63×10^{-9}s and 2.21×10^{-9}s at 295K and 4.2K, respectively.

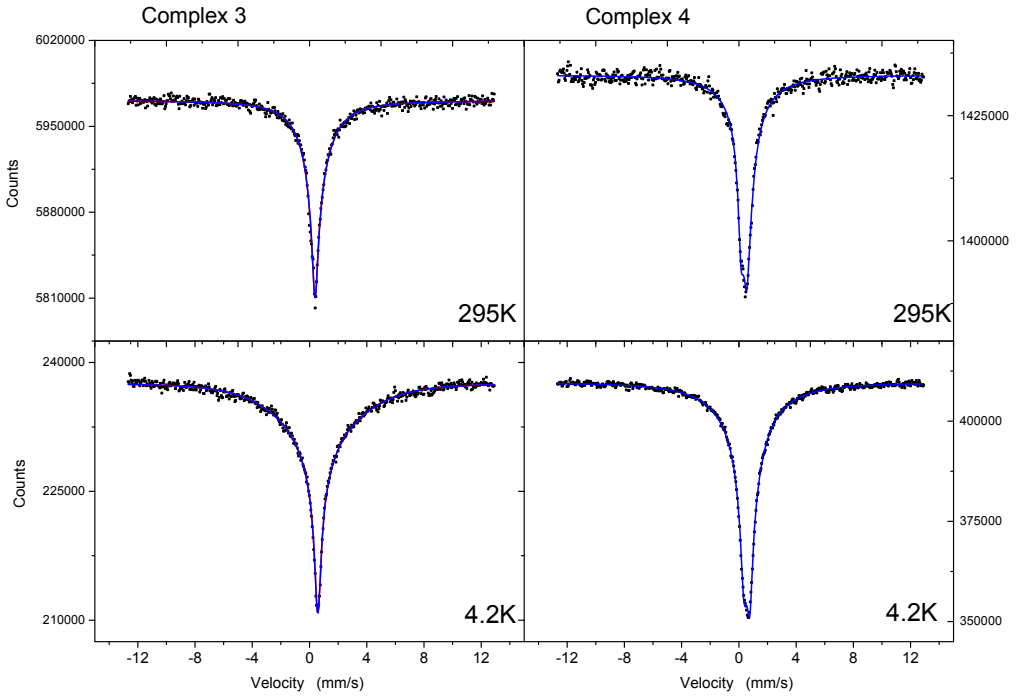

Figure 8 ^{57}Fe Mössbauer spectra of complexes **3** and **4** recorded at 295K and 4.2K.

3.4 Theoretical Modelling

ZFS parameters for high-spin PBPY-7 cations in Co(II), Fe(III), Ni(II) complexes (**1-5**), as well as for T-4 $[Co(NCS)_4]^{2-}$ and OC-6 $[Fe(NCS)_5(H_2O)]^{2-}$ have been calculated with two methods of a different nature. The first one, the post-Hartree-Fock multi-reference wavefunction approach CASSCF+NEVPT2, is considered a standard method to obtain magnetic properties[15] and calculated ZFS parameters are usually in good agreement with the experimental data. NEVPT2 is a correction to CASSCF energies due to the dynamical correlation. The second one is a hybrid methodology (LFDFT), which combines a multideterminant DFT-based method with the ligand-field theory. LFDFT includes both dynamical correlation (through the DFT exchange-correlation energy) and non-dynamical correlation (via LF Configuration Interaction). With LFDFT procedure, all customary molecular properties can be calculated,[88–94] including ZFS parameters,[19,20,95,96] however, its accuracy decreases with increasing metal-ligand covalency.[97]

Comparison between experimentally determined and calculated ZFS parameters in PBPY-7 complexes **1-5** are given in Table 1. In all cases, account of dynamic correlation introduced by NEVPT2 improves the quality of the calculated ZFS parameters at the CASSCF level of theory. Calculated principal values of the g-tensor for compounds **1-5** are also in good correspondence with experimental findings (Table S1 in SI). Weak antiferromagnetic coupling between paramagnetic centers in **2** and **4** is confirmed by calculations at B97-D/def2-TZVP level of theory (Table S2 in SI). This level of theory is proven to be suitable for the calculation of the exchange coupling via weak interactions. [98]

Table 1 Experimental and Calculated ZFS Parameters for the PBPY-7 Complexes **1**-**5**.

Complex	M	Method	D (cm^{-1})	E (cm^{-1})	E/D
1	Co(II)	SQUID	30.01	0.00	0.00
		EPR	$\|D\|>>0.3$[a]	-	0.03
		CASSCF	48.6	2.3	0.05
		CASSCF+NEVPT2	41.5	2.0	0.05
		LFDFT	47.1	2.4	0.05
2	Co(II)	SQUID	36.56	0.95	0.03
		EPR	$\|D\|>>0.3$[a]	-	0.02
		CASSCF	44.6	1.4	0.03
		CASSCF+NEVPT2	38.4	1.1	0.03
		LFDFT	43.6	2.7	0.06
3	Fe(III)	SQUID	1.57	0.12	0.08
		EPR	$\|D\|=1.67$[b]	0.17	0.10
		CASSCF	-0.2	0.01	0.05
		CASSCF+NEVPT2	-0.4	0.02	0.05
		LFDFT	-1.6	-0.4	0.24
4	Fe(III)	SQUID	-0.50	-0.01	0.04
		EPR	$\|D\|=1.57$[b]	0.16	0.10
		CASSCF[c]	-0.2/-0.2	-0.01/-0.01	0.05/0.05
		CASSCF+NEVPT2[c]	-0.3/-0.3	-0.02/-0.03	0.06/0.09
		LFDFT[c]	-1.6/-1.5	-0.4/-0.3	0.23/0.23
5	Ni(II)	SQUID	-11.71	-1.48	0.13
		EPR	$\|D\|=0.56$[b]	0.18	0.32
		CASSCF	-18.9	-3.4	0.18
		CASSCF+NEVPT2	-12.9	-2.8	0.22
		LFDFT	-7.8	-1.3	0.16

[a] Large D magnitude. [b] Sign not determined. [c] ZFS parameters for both independent heptacoordinated Fe(III) species were calculated.

In the case of Co(II) complexes (**1** and **2**), the calculated values are close to the experimental ones obtained from DC magnetic susceptibility measurements, confirming the presence of easy magnetization plane (D>0) and low rhombicity. LFDFT results are similar to the CASSCF ones. For T-4 site calculated values are: D = -1.6 cm^{-1}, E/D = 0.24 (CASSCF+NEVPT2) and D= - 4.2 cm^{-1}, E/D=0.14 (LFDFT), both in accordance with experimental findings.

In the case of Fe(III) compounds **3** and **4** calculated anisotropy parameters are much smaller compared with compounds **1** and **5**, supporting experimental findings. Calculated D values for PBPY-7 sites in **3** and **4** are very similar. For OC-6 site in **4**, calculated ZFS parameters are: D = +0.2 cm^{-1}, E/D = 0.14 (CASSCF+NEVPT2) and D=+0.3 cm^{-1}, E/D=0.06 (LFDFT). In the case of compound **3** chosen approximations fail to reproduce the correct sign of the axial ZFS parameter (Table 1). Contrary to **3**, D parameters calculated for both of the two independent heptacoordinated Fe(III) species present in crystals of compound **4** are close to the value obtained from magnetic susceptibility measurements, both in sign and in the magnitude. LFDFT gives somewhat larger values that agree well with $|D|$ from EPR. The discrepancy in sign and value of calculated and experimental D parameter of complex **3** and a simultaneously good match of these for compound **4**, indirectly give evidence the importance of long-range interactions in crystals on the magnetic anisotropy of **3**, which is not accounted in model calculations over single complex cation. Moreover, the prediction of very small ZFS parameters is still a great challenge for the exploited computational protocols.

In the case of Ni(II) compound **5**, the sign of the calculated D parameter is negative, which coincides with magnetochemistry data. These calculations also confirm that the observed X-band EPR spectrum cannot arise from complex **5** but from an impurity, e.g., octahedral Ni(II) compound. Indeed, with such a large magnitude for D, an EPR silent spectrum for complex **5** is expected. For previously magnetochemically studied heptacoordinated Ni(II) compounds significant ZFS was established with easy magnetization axis (D < 0) in the range ca. -7 to -17

cm^{-1},[32,33,35,40,43,46] In addition to our calculations (both CASSCF/NEVPT2 and LFDFT) large negative *D* value is also justified for Ni(II) compound with PBPY-7 environment by quantum-chemical calculations in Ref.[40] The Ni(II) complex has shorter M-N$_{(py)}$ and M-N$_{(imine)}$ bond lengths and significantly longer and therefore weaker M-O$_{(carbonyl)}$ bonds in comparison with those observed in the crystals of isostructural Co(II) complex (M-N$_{(py)}$ 2.015(3) Å vs. 2.188(3) Å, M-N$_{(imine)(av.)}$ 2.148(3) Å vs. 2.199(3) Å and M-O$_{(carbonyl)(av.)}$ 2.558(2) Å vs. 2.290(3) Å).[51] The Co(II) complex is more symmetrical than Ni(II) with almost equivalent in-plane Co-N (2.188(3), 2.191(3) and 2.207(3) Å) and Co-O (2.290(3) and 2.291(3) Å) bond lengths and two shorter axial Co-N$_{(isothiocyanato)}$ bonds of ~2.0 Å. The extent of distortion is confirmed with the continuous shape measures (CShMs)[99,100] calculated with SHAPE 2.1. CShM values, presenting the deviation from ideal PBPY-7 (D_{5h} symmetry) for complexes **1**-**5** are: 0.527 (**1**), 0.283 (**2**), 0.211 (**3**), 0.127 and 0.135 (**4**) and 1.009 (**5**). The largest CShM value for **5** indicates the most distorted structure. Such a distortion is the consequence of the Jahn-Teller effect[101,102] in the ideal PBPY-7 geometry (D_{5h} symmetry) of the high-spin Ni(II) complexes.[47,49] In Ni(II) complex, strongly σ-, Ni-O$_{(carbonyl)}$, antibonding orbital (Figure S8 in SI) is doubly occupied. Therefore, the Ni-O$_{(carbonyl)}$ bond cleavage and the formation of octahedral complexes is quite possible for complex **5**.[49]

The orientation of the molecules **1**, **3**, **5** in the *D*-tensor coordinate frame is shown in Figure 9. In Co(II) compound xy-plane is next to coplanar with equatorial coordination plane of the heptacoordinated metal center, the z-axis is close to the axial orientation of the metal. For Fe(III) and Ni(II) compounds with negative axial ZFS, the z-axis is collinear with the M-N$_{pyr}$ coordination bond.

The main contributions from the excited states to the magnetic anisotropy of complexes **1**-**5** are listed in the Tables S3-S6 in SI. For Co(II) complexes (**1** and **2**) all major contributions to *D* value (from 3rd and 4th exited quartet and 9th exited doublet states) are positive, resulting in

positive total D value. For complex Ni(II) complex **5** dominating negative contributions are from the 1st triplet and 4th, 5th singlet excited states, while positive contributions from 2nd and 3rd triplet and 3nd singlet states are smaller and do not compensate the total negative *D* value. For Fe(III) complexes (**3** and **4**) contributions of the excited states are much smaller, with 1st, 2nd, 16th and 17th quartet states giving a negative contribution to *D* while 12th quartet state has a positive contribution.

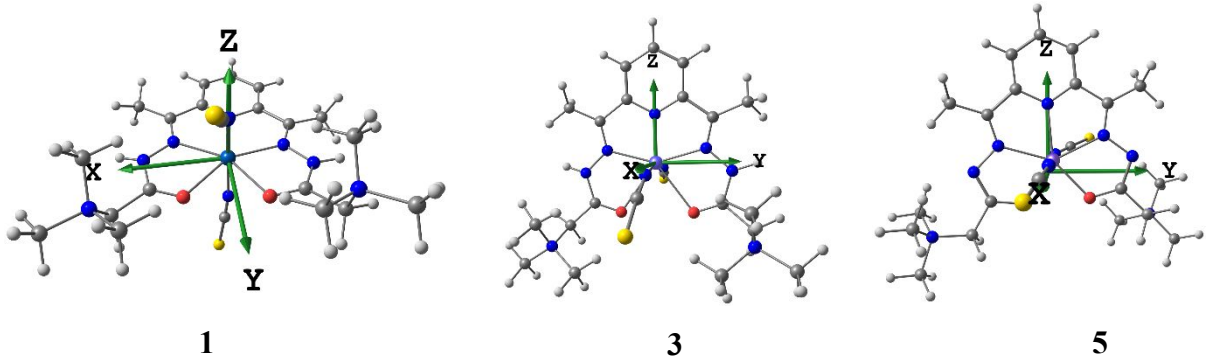

Figure 9 Orientation of the molecules in *D*-tensor frame in Co(II) (**1**), Fe(III) (**3**), and Ni(II) (**5**) complexes.

Ground electronic state of Co(II) complexes is 86% of the $|d_{xy}d_{x^2-y^2}d_{z^2}|$ determinant (see Figure 10 for MO diagram and orientation of molecular frame, Table S7 for orbital splitting as given by AI-LFT, and Table S8 for the composition of the multi-determinant wave function of the ground and selected excited states). 3rd exited quartet state is multideterminant with prevailing (46%) contribution of $|d_{yz}d_{xy}d_{z^2}|$ determinant, and it differs from the ground state by single-electron excitation $d_{yz} \rightarrow d_{x^2-y^2}$. Close in excitation energy 4th quartet state is 56% $|d_{xz}d_{xy}d_{z^2}|$ determinant and is formed mainly by single-electron excitation $d_{xz} \rightarrow d_{x^2-y^2}$. The 9th excited doublet state corresponds to flip-spin excitation from d_{xy} to $d_{x^2-y^2}$ atomic orbital.

The splitting of the d orbitals is changing from Co(II) (**1** and **2**) to Ni(II) (**5**) coordination compounds. d_{xy} orbital becomes the most stabilized one, while d_{xz} and d_{yz} are shifted by 393 and 725 cm^{-1} higher in energy, correspondingly (Table S7 in SI). These changes can be rationalized if one compares the structural parameters of **1** and **5**. Bond distances Co-NCS are 2.077 and 2.069Å, while Ni-NCS (1.997 and 1.989 Å) are c.a. 0.07 Å shorter, leading to destabilization of the d_{xz} and d_{yz} AOs when going from complex **1** to **5**. Moreover, at the same time, Co-O interatomic distances (2.222/2.196 Å) are much shorter compared to Ni-O (2.572 and 2.544 Å), which results in stabilization of the in-plane d_{xy} in Ni(II) compound. In Ni(II) complex ground state is predominantly (100%) described by a single determinant $|d_{x^2-y^2}d_{z^2}|$ (see Figure 10 and Table S8). The first triplet excited state (6752 cm^{-1}) is 100% dominated by $|d_{xy}d_{z^2}|$ (Table S8) and is due to one-electron excitation $d_{xy} \rightarrow d_{x^2-y^2}$. Consecutive 2nd and 3rd triplet excited states (8179, 9755 cm^{-1}, correspondingly) are of multideterminant nature (Table S8) and are formed by configurations 56% $d_{yz} \rightarrow d_{z^2}$ and 42% $d_{yz} \rightarrow d_{x^2-y^2}$ (2nd excited state) and 56% $d_{xz} \rightarrow d_{z^2}$ and 42% d_{xy}, $d_{yz} \rightarrow d_{z^2}, d_{x^2-y^2}$ (3rd excited state).

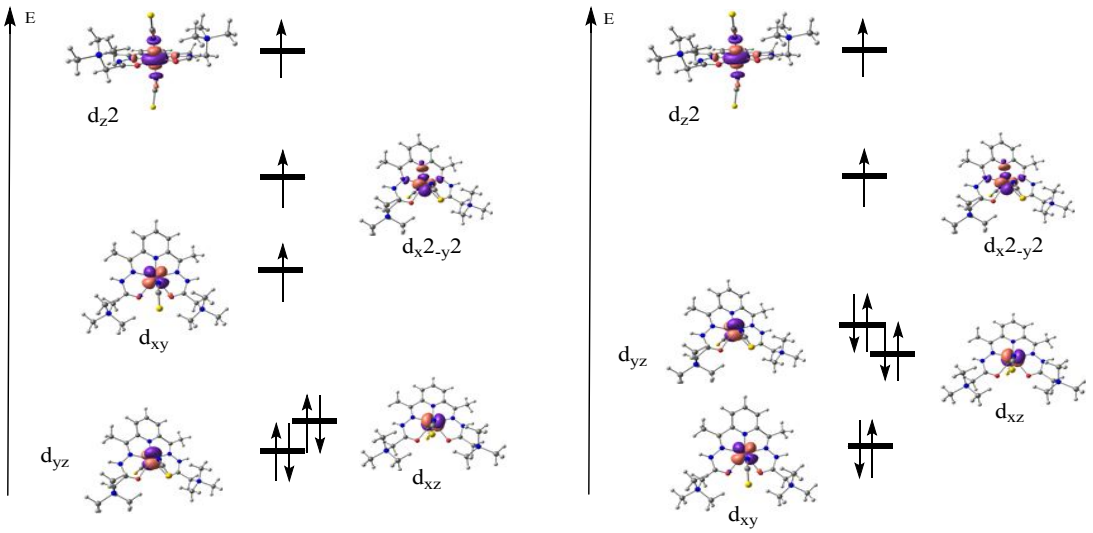

Figure 10 AI-LFT (CASSCF+NEVPT2) d-orbital splitting in Co(II) complexes **1** and **2** (left) and in Ni(II) complex **5** (right).

In the case of Fe(III) compound (**3**) the ground state is well-separated sextet, closest quartet state is 18600 cm^{-1}. That is why perturbative contributions to *D* value are rather small. According to AI-LFT, splitting of d orbitals is presented in Table S7 in SI. The lowest two LFT orbitals are next to degenerate linear combinations of d_{xz} and d_{yz} AOs orbitals: 0.54 d_{yz}+0.83 d_{xz} and 0.84 d_{yz}-0.55 d_{xz}. The first quartet excited state is dominated by 81% of $|(d_{xz})^2d_{yz}d_{x^2-y^2}d_{xy}|$ (Table S8) formed by one-electron spin-flipped transfer from the ground state $d_{z^2}\rightarrow d_{xz}$. The second quartet excited state is dominated by 83% of $|d_{xz}(d_{yz})^2d_{x^2-y^2}d_{xy}|$ formed by one-electron spin-flip transfer from the ground state $d_{z^2}\rightarrow d_{yz}$. Both excitations are close in energy due to the pseudo degeneracy of the d_{xz} and d_{yz} and give similar negative contributions to *D* value. 12th quartet state is 60% dominated by $|d_{xz}d_{yz}(d_{xy})^2d_{z^2}|$ formed by one-electron spin-flip from the ground state $d_{x^2-y^2}\rightarrow d_{xy}$ shows positive contribution to total *D* value. Close in energy 16th and 17th quartet states are dominated by 46% of $|d_{xz}d_{xy}d_{x^2-y^2}(d_{z^2})^2|$ and 45% of $|d_{yz}d_{xy}d_{x^2-y^2}(d_{z^2})^2|$ configuration, respectively, corresponding to the electron pairing one-electron excitations from d_{yz} or d_{xz} to d_{z^2}. Both excitations give a negative contribution to *D*.

3.5 Rationalization of the magnetic anisotropy in Co(II), Ni(II) and Fe(III) PBPY-7 complexes

Herein studied complexes show three distinct types of magnetic anisotropy. Co(II) complexes (**1** and **2**) show large and positive *D* values, Ni(II) (**5**) has large negative *D* value, while Fe(III) complexes (**3** and **4**) have small ZFS parameters. Magnetic anisotropy in these systems arises because the SOC mixing of the ground and certain excited states lift the degeneracy of the M_S components of the ground spin-state *S*. If the wavefunction with highest M_S becomes the ground state $D<0$, and if the ground state is with lowest M_S $D>0$. The

identification of the excited states responsible for *D* values in complexes **1**-**5** is achieved by the *ab initio* calculations described above. However, in addition to the *ab initio* quantification of the contributions of excited states to *D* values, the results can be explained using simple ligand field considerations and group theory. Selection rules for the coupling of the ground and excited states are i) direct product of the irreducible representations (irreps.) of the ground and excited states must contain the irrep of the H_{SOC} (which transform as R_x, R_y and R_z in the molecular point group); ii) ΔS=0, ±1 (i.e., in Fe(III) only quartet states can couple with the ground sextet state), iii) ΔM_s=0 (coupling via the z-component of the SOC operator, H^z_{SOC}) or ±1 (coupling via the x/y-components of the SOC operator).[21] Conditions i) and ii) are important for establishing which excited states can couple with the ground state. Using condition iii) it is possible to judge whether the SOC produces a positive or negative contribution to the total *D* value, i.e., which M_S components of the ground state will be more stabilized. Finally, *D* value is inversely proportional to the energy splitting of the ground and excited states. Thus, typically lowest energy excited states (satisfying above criteria) are most important.

Complexes **1**-**5** are of C_1 symmetry; however, we will consider higher symmetry point groups - the point group of ideal PBPY-7 coordination (D_{5h}), and its subgroup, point group of ideal $N_3O_2N_{2(ax)}$ coordination (C_{2v}). The selection rules for the higher point groups are very restrictive, but the excited states that satisfy those rules will be exactly the excited states with the largest contribution to *D* value in the real systems. The CShM values, presenting the deviation from ideal PBPY-7 (D_{5h} symmetry) for all complexes are small (0.527 (**1**), 0.283 (**2**), 0.211 (**3**), 0.127 and 0.135 (**4**) and 1.009 (**5**)) justifying this approach.

In D_{5h} point group, metal d-orbitals split into e_1'' (d_{xz}, d_{yz}), e_2' (d_{xy}, $d_{x^2-y^2}$) and a_1' (d_{z^2}), Figure 1. The ground state of Co(II) complexes in the D_{5h} point group is $^4A_2'$, of Ni(II) complexes is $^3E_2'$, and of Fe(III) complexes is $^6A_1'$. The H^z_{SOC} operator transforms as A_2' and H^{xy}_{SOC} as E_1''.

In Co(II) complexes in D_{5h} point group, lowest energy spin-allowed transition is due to the excitation from e_1'' (d_{xz}, d_{yz}) to e_2' (d_{xy}, $d_{x^2-y^2}$), leading to $^4E_1''$ and $^4E_2''$ excited states. The first one is coupled to the ground state via $H_{SOC}^{x,y}$ ($A_2' \otimes E_1'' = E_1''$), while the second one does not fulfill symmetry requirements. Because coupling through $H_{SOC}^{x,y}$ requires $\Delta Ms=\pm1$, the microstate with M_s=3/2 (M_s=-3/2) from the ground state $^4A_2'$ interacts with M_s=1/2 (M_s=-1/2) components of the excited $^4E_1''$ state. Microstate with M_s=1/2 (M_s=-1/2) from the ground state $^4A_2'$ interacts with both M_s=3/2 and M_s=-1/2 (M_s=-3/2 and M_s=1/2) microstates of $^4E_1''$. Consequently, the stabilization of M_s =±1/2 of the ground state $^4A_2'$ is larger, and hence, there is a positive contribution to the total D value from $^4E_1''$ state. Spin-flip excited state $^2A_1'$ from the ground electronic configuration, $(e_1'')^4 (e_2')^2(a_1')^1$, couples with the ground state via H_{SOC}^{z} operator ($A_2' \otimes A_1' = A_2'$). In this case, the coupling between M_s =1/2 (M_s =-1/2) components of the ground and the excited state is only possible (ΔMs=0), leading to another positive contribution to D value. When the symmetry is lowered to C_{2v}, $^4E_1''$ excited state splits into $^4B_1$ and $^4B_2$. The first one is coupled with the ground $^4A_2$ state via H_{SOC}^{y} (transforming as B_2 irrrep in C_{2v}), and the later via H_{SOC}^{x} (transforming as B_1 irrrep in C_{2v}). They have a positive contribution to D, as described above. $^2A_1'$ excited state becomes $^2A_1$ state in C_{2v}. It is coupled via H_{SOC}^{z} operator and it gives a positive contribution to D value. These three excited states correspond exactly to the three most important excited states for the D value of complexes **1** and **2**, as found by *ab initio* calculations. Interestingly, $^4E_2''$ excited state in D_{5h}, which does not contribute to the ZFS in D_{5h}, in C_{2v} symmetry splits into $^4B_1$ and $^4B_2$. These two states also give a positive contribution to D (once symmetry is lowered). However, their contribution is lower than of the states (with the same symmetry), but that originate from $^4E_1''$. This is confirmed by *ab initio* calculations (1st and 2nd quartet states correlate with $^4E_2''$, while 3rd and 4th correlate with $^4E_1''$, Tables S3 and S4 in SI for *ab initio* calculated contributions).

The ground state of Ni(II) complexes in the D_{5h} point group is $^3E_2'$. Because of the orbital degeneracy, magnetic anisotropy exists mostly due to the in-state SOC.[20] The situation is completely analogous to the Ni(II) in trigonal bipyramidal coordination.[19] The microstates within the $^3E_2'$ term are coupled by H^z_{SOC} operator and are split into three groups of double degenerate states. The spin reversal barrier in D_{5h} symmetry, i.e., splitting between these states is equal to the SOC constant of Ni(II). If considering covalency and influence of the excited states (in particular the first excited $^3E_1''$ state, excitation from e_1'' to e_2') this barrier will be lower, but still very large (ca. 500 cm^{-1}). However, orbitally degenerate systems, like Ni(II) complexes in D_{5h} point group, are subject to the Jahn-Teller distortion.[101,102] The system is stabilized by lowering the symmetry to C_{2v}, and the degenerate levels split. $^3E_2'$ ground state splits into $^3A_1$ and $^3A_2$. The magnetic anisotropy will be lower than in higher symmetry.[19] Since the partially filled degenerate orbitals in D_{5h} are d_{xy} and $d_{x^2-y^2}$ (e_2' set), the distortion will be mainly located in the equatorial plane. Regarding the structure of complex **5**, because of double occupancy of d_{xy} orbital (see Figure 10 for the orientation of the molecular frame), and its metal-ligand σ-antibonding nature (Figure S8 in SI), stabilization of the system is achieved with the elongation of corresponding Ni-equatorial ligand distances. The ground state in C_{2v}, when d_{xy} orbital is doubly occupied, is $^3A_1$. The main source of the magnetic anisotropy in C_{2v} symmetry is the SOC coupling of the Jahn-Teller split states, i.e., SOC coupling of the $^3A_1$ and $^3A_2$ states via H^z_{SOC}. The M_s=1 (M_s=-1) microstate of the ground $^3A_1$ state interacts with the M_s=1 (M_s=-1) component of the $^3A_2$ excited state and M_s=0 microstate of the ground $^3A_1$ state interacts with the M_s=0 of the excited state (ΔM_s=0). Because coupling is larger for larger $|S_z|$ the SOC between $^3A_1$ and $^3A_2$ states leads to the negative D value. As seen from *ab initio* calculations, this, $d_{xy} \rightarrow d_{x^2-y^2}$, transition gives dominating negative contribution to D in complex **5**. $^3E_1''$ excited state in D_{5h} (excitation from e_1'' to e_2') splits into $^3B_1$ and $^3B_2$. These excited states couple with the ground state through H^y_{SOC} and H^x_{SOC}, respectively, and because

of $\Delta Ms=\pm1$ rule have a positive contribution to *D*. Analogous situation is with excitation from e_1'' to a_1'. Concerning the singlet states, lowest-lying is $^1E_2'$ (spin-flip within the ground electronic configuration) that splits into $^1A_1$ and $^1A_2$ states in C_{2v}. $^1A_2$ state couples with the ground state via H^z_{SOC}, and only $M_s=0$ microstates interact ($\Delta M_s=0$) leading also to the positive contribution to *D*. On the contrary, singlet states arising from e_1'' to e_2' excitation ($^1E_1''$ that splits into $^1B_1$ and $^1B_2$) have negative contribution to *D*. It should be pointed out that because the primary source of the ZFS in Ni(II) PBPY-7 complexes is the SOC of the Jahn-Teller split states (relatively small energy separation between states), these systems tend to have negative *D*. However, as distortion is larger, influence of the excited states with positive contribution to *D* will be more important. As seen from *ab initio* calculations in complex **5**, the contribution of the first triplet state is -64 cm^{-1} (Table S6 in SI). Excited states with positive contributions compensate to some extent this negative *D* value, giving the total *D* of -13 cm^{-1}.

The ground state of Fe(III) complexes in the D_{5h} point group is $^6A_1'$. Because of the isotropic nature of the ground state, ZFS is expected to be small. Furthermore, there are no low-lying excited states that can considerably contribute to the splitting of this six-fold degenerate multiplet. In D_{5h} H^z_{SOC} couples ground state and $^4A_2'$ excited states, while H^{xy}_{SOC} couples ground and $^4E_1''$ states. Because of $\Delta M_s=0$ rule, $M_s=\pm3/2$ and $M_s=\pm1/2$ microstates of the ground $^6A_1'$ couple with corresponding microstates of $^4A_2'$, while $M_s=\pm5/2$ microstates do not interact. Ordering of the spin-orbit split states must be either $\pm5/2, \pm3/2, \pm1/2$ ($D<0$) or $\pm1/2, \pm3/2, \pm5/2$ ($D>0$), therefore, stabilization of $M_s=\pm1/2$ microstates of the ground $^6A_1'$ is larger than stabilization of $M_s=\pm3/2$ microstates. In other words, $^4A_2'$ states bring a positive contribution to *D* value. Similarly, $^4E_1''$ states, taking into account $\Delta Ms=\pm1$ rule and energy order of the microstates, give negative contribution to *D*. In C_{2v} symmetry, $^4B_1$ and $^4B_2$ excited states are giving negative, while $^4A_2$ gives positive contribution to *D*. As shown by *ab initio* calculations for complexes **3** and **4**, lowest quartet states are $d_z^2 \rightarrow d_{xz}$ ($^4B_1$ in C_{2v}) and $d_z^2 \rightarrow d_{yz}$ ($^4B_2$ in C_{2v}),

that bring negative contributions to *D* value. They correlate to $^4E_1''$ state in ideal D_{5h} symmetry. The higher-lying excitations, from d_{yz} or d_{xz} to d_z^2 also correlate to $^4E_1''$ (spin-flip from e_1'' to a_1') and bring negative contribution to *D*. $d_{x^2-y^2} \rightarrow d_{xy}$ excitation correlates to $^4A_2'$ (spin-flip within e_2' set) and gives a positive contribution to *D*.

4. CONCLUSIONS

The complexes of 2,2′-[2,6-pyridinediylbis(ethylidyne-1-hydrazinyl-2-ylidene)]bis[*N*,*N*,*N*-trimethyl-2-oxoethanaminium] ligand with Co(II), Fe(III) and Ni(II) in PBPY-7 environment have been analyzed by magnetic susceptibility measurements, powder X-band EPR spectroscopy, and Mössbauer spectroscopy (for Fe(III) complexes). Results showed that all complexes are high spin and display distinct magnetic anisotropy. The ZFS in these complexes is validated and rationalized by CASSCF+NEVPT2 and LFDFT calculations. Consistency between the two different computational methods confirms the reliability of the results. These complexes display three distinct types of magnetic anisotropy. Co(II) complexes (**1** and **2**) show large and positive *D* values (ca. +30 cm^{-1} and *E/D*=0). Ni(II) complex (**5**) has negative *D* value (ca. -12 cm^{-1}). Fe(III) complexes have small ZFS parameters (for **3** *D*= +1.5 cm^{-1} and for **4** *D*= -0.5 cm^{-1}).

Origin of the magnetic anisotropy in these systems is mixing of the ground and a small number of excited states through SOC. *Ab initio* calculations were used to pinpoint the most important excitations. These excitations are a consequence of the electronic structure of the central metal ion in ideal PBPY-7 coordination (D_{5h} point group). In Co(II) complexes **1** and **2** positive *D* is a consequence of spin-allowed e_1'' (d_{xz}, d_{yz}) to e_2' (d_{xy}, $d_{x^2-y^2}$) transition and spin-flip within the ground electronic configuration (d_{xy}, to $d_{x^2-y^2}$). In Ni(II) complex **5** negative *D* is due to the $d_{xy} \rightarrow d_{x^2-y^2}$ excitation. The importance of this excitation can be traced back to the

unquenched orbital angular momentum and the Jahn-Teller effect in Ni(II) complexes with ideal D_{5h} symmetry. Spin-allowed excitation from e_1'' to e_2' counterbalance in a certain degree negative contribution of $d_{xy} \rightarrow d_{x^2-y^2}$ excitation, lowering the negative magnitude of *D* in **5**. Differently to the Co(II) and Ni(II) complexes, in Fe(III) complexes, there are no low-lying excited states, and hence all the contributions to ZFS are small. In Fe(III) complexes, quartet states arising from a_1' (d_{z^2}) to e_1'' (d_{xz}, d_{yz}) transition and from e_1'' to a_1' transition are giving negative contribution to *D*, while spin-flip $d_{x^2-y^2} \rightarrow d_{xy}$ (spin-flip within e_2' set) gives positive contribution to *D*. A balance between these opposite trends yields the overall small *D* value.

Knowledge of the specific excitations that govern the sign and magnitude of the ZFS parameter, *D,* can be used to control and engineer the magnetic anisotropy in transition metal complexes. For example, in Co(II) PBPY-7 complexes, choice of weaker field ligands in the equatorial plane would stabilize d_{xy}, $d_{x^2-y^2}$ orbitals. That would make smaller energy difference between e_1'' (d_{xz}, d_{yz}) and e_2' (d_{xy}, $d_{x^2-y^2}$) orbitals leading to larger positive *D*. Stronger π-donors in axial position would raise the energy of the e_1'' set, that would be beneficial for making larger positive *D*. More symmetrical chelate ligand in the equatorial plane would also lead to more positive *D,* because of smaller separation between d_{xy} and $d_{x^2-y^2}$ orbitals (lowering the energy of the spin-flip d_{xy} to $d_{x^2-y^2}$ excitations). For Ni(II), it is necessary to use systems that are as close as possible to the ideal D_{5h} symmetry. Using symmetric and rigid ligands in the equatorial plane and bulky axial ligands could lead to the suppression of the (pseudo) Jahn-Teller distortion. By careful choice of ligands, Ni(II) complexes in PBPY-7 environment could show very large magnetic anisotropy, similarly to the trigonal bipyramidal $[NiCl_3(Hdabco)_2]^+$ (dabco is 1,4-diazabicyclo[2.2.2]-octane).[19] Unquestionably, this will be a formidable and challenging task because of difficulties in making PBPY-7 Ni(II) complexes in a first place. High spin Fe(III) complexes are not expected to have large ZFS because of the ground $^6A_1'$

state. Additionally, there are no close-lying excited states that could be effectively tuned to significantly rise the magnetic anisotropy. Studies of magneto-structural correlations and possible modifications of PBPY-7 complexes are ongoing.

ASSOCIATED CONTENT

Supporting Information. Comparison of EPR spectra of **1** and **2** (Figure S1); Additional Mössbauer spectra (Figures S2-S5); Kohn-Sham molecular orbitals with dominant metal d character (Figures S6-S8); Calculated principal components of g-tensor (Table S1); Calculated J values (Table S2); Transition energies and contributions of excited states to *D* and *E* (Tables S3-S6); d-Orbitals splitting according to AI-LFT (Table S7); Composition of multi-determinant wave function of the ground and selected excited states (Table S8).

AUTHOR INFORMATION

Corresponding Authors

*bozidar@chem.bg.ac.rs (Božidar Čobeljić)

*matijaz@chem.bg.ac.rs; matija.zlatar@ihtm.bg.ac.rs (Matija Zlatar)

Author Contributions

The manuscript was written through contributions of all authors. All authors have given approval to the final version of the manuscript.

ACKNOWLEDGMENT

This work was supported by the Ministry of Education, Science and Technological Development of the Republic of Serbia (Grants OI 172035 and OI 172055), the Slovenian Research Agency (P-0175 and P1-0112) and is supported by Southern Federal University.

REFERENCES

(1) Kahn, O. *Molecular magnetism*; VCH Publishers, 1993.

(2) Miller, J. S.; Gatteschi, D. Molecule-based magnets. *Chem. Soc. Rev.* **2011**, *40* (6), 3065–3066 DOI: 10.1039/c1cs90019f.

(3) Ferrando-Soria, J.; Vallejo, J.; Castellano, M.; Martínez-Lillo, J.; Pardo, E.; Cano, J.; Castro, I.; Lloret, F.; Ruiz-García, R.; Julve, M. Molecular magnetism, quo vadis? A historical perspective from a coordination chemist viewpoint☆. *Coord. Chem. Rev.* **2017**, *339*, 17–103 DOI: 10.1016/J.CCR.2017.03.004.

(4) Meng, Y.-S.; Jiang, S.-D.; Wang, B.-W.; Gao, S. Understanding the magnetic anisotropy toward single-ion magnets. *Acc. Chem. Res.* **2016**, *49* (11), 2381–2389 DOI: 10.1021/acs.accounts.6b00222.

(5) Troiani, F.; Affronte, M. Molecular spins for quantum information technologies. *Chem. Soc. Rev.* **2011**, *40* (6), 3119–3129 DOI: 10.1039/c0cs00158a.

(6) Stamp, P. C. E.; Gaita-Ariño, A. Spin-based quantum computers made by chemistry: hows and whys. *J. Mater. Chem.* **2009**, *19* (12), 1718–1730 DOI: 10.1039/B811778K.

(7) Winpenny, R. E. P. Quantum information processing using molecular nanomagnets as qubits. *Angew. Chemie Int. Ed.* **2008**, *47* (42), 7992–7994 DOI: 10.1002/anie.200802742.

(8) Bogani, L.; Wernsdorfer, W. Molecular spintronics using single-molecule magnets. *Nat. Mater.* **2008**, *7* (3), 179–186 DOI: 10.1038/nmat2133.

(9) Ding, Y.-S.; Deng, Y.-F.; Zheng, Y.-Z.; Ding, Y.-S.; Deng, Y.-F.; Zheng, Y.-Z. The rise of single-ion magnets as spin qubits. *Magnetochemistry* **2016**, *2* (4), 40 DOI: 10.3390/magnetochemistry2040040.

(10) Gómez-Coca, S.; Aravena, D.; Morales, R.; Ruiz, E. Large magnetic anisotropy in mononuclear metal complexes. *Coord. Chem. Rev.* **2015**, *289–290*, 379–392 DOI: 10.1016/J.CCR.2015.01.021.

(11) Boča, R. Zero-field splitting in metal complexes. *Coord. Chem. Rev.* **2004**, *248* (9–10), 757–815 DOI: 10.1016/j.ccr.2004.03.001.

(12) Waldmann, O. A criterion for the anisotropy barrier in single-molecule magnets. **2007**, *46* (24), 10035–10037 DOI: 10.1021/IC701365T.

(13) Neese, F.; Pantazis, D. A. What is not required to make a single molecule magnet. *Faraday Discuss.* **2011**, *148* (0), 229–238 DOI: 10.1039/C005256F.

(14) Bar, A. K.; Pichon, C.; Sutter, J.-P. Magnetic anisotropy in two- to eight-coordinated transition–metal complexes: recent developments in molecular magnetism. *Coord. Chem. Rev.* **2016**, *308*, 346–380 DOI: 10.1016/J.CCR.2015.06.013.

(15) Atanasov, M.; Aravena, D.; Suturina, E.; Bill, E.; Maganas, D.; Neese, F. First principles approach to the electronic structure, magnetic anisotropy and spin relaxation in mononuclear 3d-transition metal single molecule magnets. *Coord. Chem. Rev.* **2015**, *289–290*, 177–214 DOI: 10.1016/J.CCR.2014.10.015.

(16) Gomez-Coca, S.; Cremades, E.; Aliaga-Alcalde, N.; Ruiz, E. Mononuclear single-molecule magnets: tailoring the magnetic anisotropy of first-row transition-metal complexes. *J. Am. Chem. Soc.* **2013**, *135* (18), 7010–7018 DOI: 10.1021/ja4015138.

(17) Cirera, J.; Ruiz, E.; Alvarez, S.; Neese, F.; Kortus, J. How to build molecules with large magnetic anisotropy. *Chem. - A Eur. J.* **2009**, *15* (16), 4078–4087 DOI: 10.1002/chem.200801608.

(18) Chibotaru, L. F. Theoretical understanding of anisotropy in molecular nanomagnets. In *Molecular Nanomagnets and Related Phenomena*; Song, G., Ed.; Springer, Berlin, Heidelberg, 2014; pp 185–229.

(19) Gruden-Pavlović, M.; Perić, M.; Zlatar, M.; García-Fernández, P. Theoretical study of the magnetic anisotropy and magnetic tunnelling in mononuclear Ni(II) complexes with potential molecular magnet behavior. *Chem. Sci.* **2014**, *5* (4), 1453–1462 DOI: 10.1039/C3SC52984C.

(20) Perić, M.; García-Fuente, A.; Zlatar, M.; Daul, C.; Stepanović, S.; García-Fernández, P.; Gruden-Pavlović, M. Magnetic anisotropy in "scorpionate" first-row transition-metal complexes: a theoretical investigation. *Chem. - A Eur. J.* **2015**, *21* (9), 3716–3726 DOI: 10.1002/chem.201405480.

(21) Cahier, B.; Maurice, R.; Bolvin, H.; Mallah, T.; Guihéry, N.; Cahier, B.; Maurice, R.; Bolvin, H.; Mallah, T.; Guihéry, N. Tools for predicting the nature and magnitude of magnetic anisotropy in transition metal complexes: application to Co(II) complexes. *Magnetochemistry* **2016**, *2* (3), 31 DOI: 10.3390/magnetochemistry2030031.

(22) Craig, G. A.; Murrie, M. 3d single-ion magnets. *Chemical Society Reviews*. Royal Society of Chemistry April 21, 2015, pp 2135–2147.

(23) Duboc, C. Determination and prediction of the magnetic anisotropy of Mn ions. *Chem. Soc. Rev.* **2016**, *45* (21), 5834–5847 DOI: 10.1039/C5CS00898K.

(24) Zadrozny, J. M.; Xiao, D. J.; Atanasov, M.; Long, G. J.; Grandjean, F.; Neese, F.; Long, J. R. Magnetic blocking in a linear iron(I) complex. *Nat. Chem.* **2013**, *5* (7), 577–581 DOI: 10.1038/nchem.1630.

(25) Yao, X.-N.; Du, J.-Z.; Zhang, Y.-Q.; Leng, X.-B.; Yang, M.-W.; Jiang, S.-D.; Wang, Z.-X.; Ouyang, Z.-W.; Deng, L.; Wang, B.-W.; et al. Two-coordinate Co(II) imido complexes as outstanding single-molecule magnets. *J. Am. Chem. Soc.* **2017**, *139* (1), 373–380 DOI: 10.1021/jacs.6b11043.

(26) Bunting, P. C.; Atanasov, M.; Damgaard-Møller, E.; Perfetti, M.; Crassee, I.; Orlita, M.; Overgaard, J.; van Slageren, J.; Neese, F.; Long, J. R. A linear cobalt(II) complex with maximal orbital angular momentum from a non-aufbau ground state. *Science* **2018**, *362* (6421), eaat7319 DOI: 10.1126/science.aat7319.

(27) Platas-Iglesias, C.; Vaiana, L.; Esteban-Gómez, D.; Avecilla, F.; Real, J. A.; Blas, A. de; Rodríguez-Blas, T. Electronic structure study of seven-coordinate first-row transition metal complexes derived from 1,10-diaza-15-crown-5: a successful marriage of theory with experiment. *Inorg. Chem.* **2005**, *44*, 9704–9713 DOI: 10.1021/IC051119H.

(28) Batchelor, L. J.; Sangalli, M.; Guillot, R.; Guihéry, N.; Maurice, R.; Tuna, F.; Mallah, T. Pentanuclear cyanide-bridged complexes based on highly anisotropic CoII seven-coordinate building blocks: synthesis, structure, and magnetic behavior. *Inorg. Chem.* **2011**, *50* (23), 12045–12052 DOI: 10.1021/ic201534e.

(29) Drahoš, B.; Herchel, R.; Trávníček, Z. Impact of halogenido coligands on magnetic anisotropy in seven-coordinate Co(II) complexes. *Inorg. Chem.* **2017**, *56* (9), 5076–5088 DOI: 10.1021/acs.inorgchem.7b00235.

(30) Shao, D.; Zhou, Y.; Pi, Q.; Shen, F.-X.; Yang, S.-R.; Zhang, S.-L.; Wang, X.-Y. Two-dimensional frameworks formed by pentagonal bipyramidal cobalt(II) ions and hexacyanometallates: antiferromagnetic ordering, metamagnetism and slow magnetic relaxation. *Dalt. Trans.* **2017**, *46* (28), 9088–9096 DOI: 10.1039/C7DT01893B.

(31) Mondal, A. K.; Mondal, A.; Dey, B.; Konar, S. Influence of the coordination environment on easy-plane magnetic anisotropy of pentagonal bipyramidal cobalt(II) complexes. *Inorg. Chem.* **2018**, *57* (16), 9999–10008 DOI:

10.1021/acs.inorgchem.8b01162.

(32) Antal, P.; Drahoš, B.; Herchel, R.; Trávníček, Z. Structure and magnetism of seven-coordinate FeIII , FeII , CoII and NiII complexes containing a heptadentate 15-membered pyridine-based macrocyclic ligand. *Eur. J. Inorg. Chem.* **2018**, *2018* (38), 4286–4297 DOI: 10.1002/ejic.201800769.

(33) Deng, Y.-F.; Yao, B.; Zhan, P.-Z.; Gan, D.; Zhang, Y.-Z.; Dunbar, K. R. Synthesis and magnetic studies of pentagonal bipyramidal metal complexes of Fe, Co and Ni. *Dalt. Trans.* **2019**, *48* (10), 3243–3248 DOI: 10.1039/C8DT05074K.

(34) Mondal, A.; Kharwar, A. K.; Konar, S. Sizeable effect of lattice solvent on field induced slow magnetic relaxation in seven coordinated Co(II) complexes. *Inorg. Chem.* **2019**, *58* (16), 10686–10693 DOI: 10.1021/acs.inorgchem.9b00615.

(35) Bar, A. K.; Gogoi, N.; Pichon, C.; Goli, V. M. L. D. P.; Thlijeni, M.; Duhayon, C.; Suaud, N.; Guihéry, N.; Barra, A.-L.; Ramasesha, S.; et al. Pentagonal bipyramid FeII complexes: robust Ising-spin units towards heteropolynuclear nanomagnets. *Chem. - A Eur. J.* **2017**, *23* (18), 4380–4396 DOI: 10.1002/chem.201605549.

(36) Bartolomé, E.; Alonso, P. J.; Arauzo, A.; Luzón, J.; Bartolomé, J.; Racles, C.; Turta, C. Magnetic properties of the seven-coordinated nanoporous framework material Co(bpy)1.5 (NO3)2 (bpy = 4,4′-bipyridine). *Dalt. Trans.* **2012**, *41* (34), 10382–10389 DOI: 10.1039/C2DT31135F.

(37) Higgins, R. F.; Livesay, B. N.; Ozumerzifon, T. J.; Joyce, J. P.; Rappé, A. K.; Shores, M. P. A family of related Co(II) terpyridine compounds exhibiting field induced single-molecule magnet properties. *Polyhedron* **2018**, *143*, 193–200 DOI: 10.1016/j.poly.2017.10.008.

(38) Wang, J.; Cui, H. H.; Zhang, Y. Q.; Chen, L.; Chen, X. T. Magnetic anisotropy and slow magnetic relaxation of seven-coordinate cobalt(II)–nitrate complexes. *Polyhedron* **2018**, *154*, 148–155 DOI: 10.1016/j.poly.2018.07.050.

(39) Schleife, F.; Rodenstein, A.; Kirmse, R.; Kersting, B. Seven-coordinate Mn(II) and Co(II) complexes of the pentadentate ligand 2,6-diacetyl-4-carboxymethyl-pyridine bis(benzoylhydrazone): synthesis, crystal structure and magnetic properties. *Inorganica Chim. Acta* **2011**, *374* (1), 521–527 DOI: 10.1016/J.ICA.2011.02.064.

(40) Ruamps, R.; Batchelor, L. J.; Maurice, R.; Gogoi, N.; Jiménez-Lozano, P.; Guihéry, N.; de Graaf, C.; Barra, A.-L.; Sutter, J.-P.; Mallah, T. Origin of the magnetic anisotropy in heptacoordinate Ni II and Co II complexes. *Chem. - A Eur. J.* **2013**, *19* (3), 950–956 DOI: 10.1002/chem.201202492.

(41) Huang, X.-C.; Zhou, C.; Shao, D.; Wang, X.-Y. Field-induced slow magnetic relaxation in cobalt(II) compounds with pentagonal bipyramid geometry. *Inorg. Chem.* **2014**, *53* (24), 12671–12673 DOI: 10.1021/ic502006s.

(42) Chen, L.; Chen, S.-Y.; Sun, Y.-C.; Guo, Y.-M.; Yu, L.; Chen, X.-T.; Wang, Z.; Ouyang, Z. W.; Song, Y.; Xue, Z.-L. Slow magnetic relaxation in mononuclear seven-coordinate cobalt(II) complexes with easy plane anisotropy. *Dalt. Trans.* **2015**, *44* (25), 11482–11490 DOI: 10.1039/C5DT00785B.

(43) Drahoš, B.; Herchel, R.; Trávníček, Z. Structural, magnetic, and redox diversity of first-row transition metal complexes of a pyridine-based macrocycle: well-marked trends supported by theoretical DFT calculations. *Inorg. Chem.* **2015**, *54* (7), 3352–3369 DOI: 10.1021/ic503054m.

(44) Shao, D.; Zhang, S.-L.; Shi, L.; Zhang, Y.-Q.; Wang, X.-Y. Probing the effect of axial

ligands on easy-plane anisotropy of pentagonal-bipyramidal cobalt(II) single-ion magnets. *Inorg. Chem.* **2016**, *55* (21), 10859–10869 DOI: 10.1021/acs.inorgchem.6b00854.

(45) Dey, M.; Dutta, S.; Sarma, B.; Deka, R. C.; Gogoi, N. Modulation of the coordination environment: a convenient approach to tailor magnetic anisotropy in seven coordinate Co(II) complexes. *Chem. Commun.* **2016**, *52* (4), 753–756 DOI: 10.1039/C5CC07397A.

(46) Antal, P.; Drahoš, B.; Herchel, R.; Trávníček, Z. Late first-row transition-metal complexes containing a 2-pyridylmethyl pendant-armed 15-membered macrocyclic ligand. Field-induced slow magnetic relaxation in a seven-coordinate cobalt(II) compound. *Inorg. Chem.* **2016**, *55* (12), 5957–5972 DOI: 10.1021/acs.inorgchem.6b00415.

(47) Regueiro-Figueroa, M.; Lima, L. M. P.; Blanco, V.; Esteban-Gómez, D.; de Blas, A.; Rodríguez-Blas, T.; Delgado, R.; Platas-Iglesias, C. Reasons behind the relative abundances of heptacoordinate complexes along the late first-row transition metal series. *Inorg. Chem.* **2014**, *53* (24), 12859–12869 DOI: 10.1021/ic501869y.

(48) Gogoi, N.; Thlijeni, M.; Duhayon, C.; Sutter, J.-P. Heptacoordinated nickel(II) as an Ising-type anisotropic building unit: illustration with a pentanuclear [(NiL)3{W(CN)8}2] complex. *Inorg. Chem.* **2013**, *52* (5), 2283–2285 DOI: 10.1021/ic3027368.

(49) Stepanović, S.; Andjelković, L.; Zlatar, M.; Andjelković, K.; Gruden-Pavlović, M.; Swart, M. Role of Spin State and Ligand Charge in Coordination Patterns in Complexes of 2,6-Diacetylpyridinebis(semioxamazide) with 3d-Block Metal Ions: A Density Functional Theory Study. *Inorg. Chem.* **2013**, *52* (23), 13415–13423 DOI:

10.1021/ic401752n.

(50) Popov, L. D.; Morozov, A. N.; Shcherbakov, I. N.; Tupolova, Y. P.; Lukov, V. V; Kogan, V. A. Metal complexes with polyfunctional ligands based of bis(hydrazones) of dicarbonyl compounds. *Russ. Chem. Rev.* **2009**, *78* (7), 643–658 DOI: 10.1070/RC2009v078n07ABEH003890.

(51) Brađan, G.; Čobeljić, B.; Pevec, A.; Turel, I.; Milenković, M.; Radanović, D.; Šumar-Ristović, M.; Adaila, K.; Milenković, M.; Anđelković, K. Synthesis, characterization and antimicrobial activity of pentagonal-bipyramidal isothiocyanato Co(II) and Ni(II) complexes with 2,6-diacetylpyridine bis(trimethylammoniumacetohydrazone). *J. Coord. Chem.* **2016**, *69* (5), 801–811 DOI: 10.1080/00958972.2016.1139702.

(52) Anđelković, K.; Milenković, M. R.; Pevec, A.; Turel, I.; Matić, I. Z.; Vujčić, M.; Sladić, D.; Radanović, D.; Brađan, G.; Belošević, S.; et al. Synthesis, characterization and crystal structures of two pentagonal-bipyramidal Fe(III) complexes with dihydrazone of 2,6-diacetylpyridine and Girard's T reagent. Anticancer properties of various metal complexes of the same ligand. *J. Inorg. Biochem.* **2017**, *174*, 137–149 DOI: 10.1016/J.JINORGBIO.2017.06.011.

(53) Chilton, N. F.; Anderson, R. P.; Turner, L. D.; Soncini, A.; Murray, K. S. PHI: A powerful new program for the analysis of anisotropic monomeric and exchange-coupled polynuclear *d* - and *f* -block complexes. *J. Comput. Chem.* **2013**, *34* (13), 1164–1175 DOI: 10.1002/jcc.23234.

(54) Stoll, S.; Schweiger, A. EasySpin, a comprehensive software package for spectral simulation and analysis in EPR. *J. Magn. Reson.* **2006**, *178* (1), 42–55 DOI: 10.1016/J.JMR.2005.08.013.

(55) Roos, B. O.; Taylor, P. R.; Siegbahn, P. E. M. A complete active space SCF method (CASSCF) using a density matrix formulated super-CI approach. *Chem. Phys.* **1980**, *48* (2), 157–173 DOI: 10.1016/0301-0104(80)80045-0.

(56) Siegbahn, P.; Heiberg, A.; Roos, B.; Levy, B. A comparison of the super-CI and the Newton-Raphson scheme in the complete active space SCF method. *Phys. Scr.* **1980**, *21* (3–4), 323–327 DOI: 10.1088/0031-8949/21/3-4/014.

(57) Siegbahn, P. E. M.; Almlöf, J.; Heiberg, A.; Roos, B. O. The complete active space SCF (CASSCF) method in a Newton–Raphson formulation with application to the HNO molecule. *J. Chem. Phys.* **1981**, *74* (4), 2384–2396 DOI: 10.1063/1.441359.

(58) Angeli, C.; Cimiraglia, R.; Evangelisti, S.; Leininger, T.; Malrieu, J.-P. Introduction of n-electron valence states for multireference perturbation theory. *J. Chem. Phys.* **2001**, *114* (23), 10252–10264 DOI: 10.1063/1.1361246.

(59) Angeli, C.; Cimiraglia, R.; Malrieu, J.-P. N-electron valence state perturbation theory: a fast implementation of the strongly contracted variant. *Chem. Phys. Lett.* **2001**, *350* (3–4), 297–305 DOI: 10.1016/S0009-2614(01)01303-3.

(60) Angeli, C.; Cimiraglia, R. Multireference perturbation configuration interaction V. Third-order energy contributions in the Moeller-Plesset and Epstein-Nesbet partitions. *Theor. Chem. Accounts Theory, Comput. Model. (Theoretica Chim. Acta)* **2002**, *107* (5), 313–317 DOI: 10.1007/s00214-002-0336-z.

(61) Angeli, C.; Cimiraglia, R.; Malrieu, J.-P. N-electron valence state perturbation theory: a spinless formulation and an efficient implementation of the strongly contracted and of the partially contracted variants. *J. Chem. Phys.* **2002**, *117* (20), 9138–9153 DOI: 10.1063/1.1515317.

(62) Neese, F. The ORCA program system. *Wiley Interdiscip. Rev. Comput. Mol. Sci.* **2012**, *2* (1), 73–78 DOI: 10.1002/wcms.81.

(63) Neese, F. Software update: the ORCA program system, version 4.0. *Wiley Interdiscip. Rev. Comput. Mol. Sci.* **2018**, *8* (1), e1327 DOI: 10.1002/wcms.1327.

(64) Hess, B. A. Relativistic electronic-structure calculations employing a two-component no-pair formalism with external-field projection operators. *Phys. Rev. A* **1986**, *33* (6), 3742–3748 DOI: 10.1103/PhysRevA.33.3742.

(65) Pantazis, D. A.; Chen, X.-Y.; Landis, C. R.; Neese, F. All-Electron Scalar Relativistic Basis Sets for Third-Row Transition Metal Atoms. *J. Chem. Theory Comput.* **2008**, *4* (6), 908–919 DOI: 10.1021/ct800047t.

(66) Schäfer, A.; Horn, H.; Ahlrichs, R. Fully optimized contracted Gaussian basis sets for atoms Li to Kr. *J. Chem. Phys.* **1992**, *97* (4), 2571–2577 DOI: 10.1063/1.463096.

(67) Schäfer, A.; Huber, C.; Ahlrichs, R. Fully optimized contracted Gaussian basis sets of triple zeta valence quality for atoms Li to Kr. *J. Chem. Phys.* **1994**, *100* (8), 5829–5835 DOI: 10.1063/1.467146.

(68) Weigend, F.; Ahlrichs, R. Balanced basis sets of split valence, triple zeta valence and quadruple zeta valence quality for H to Rn: design and assessment of accuracy. *Phys. Chem. Chem. Phys.* **2005**, *7* (18), 3297–3305 DOI: 10.1039/b508541a.

(69) Neese, F. An improvement of the resolution of the identity approximation for the formation of the Coulomb matrix. *J. Comput. Chem.* **2003**, *24* (14), 1740–1747 DOI: 10.1002/jcc.10318.

(70) Ganyushin, D.; Neese, F. First-principles calculations of zero-field splitting parameters.

J. Chem. Phys. **2006**, *125* (2), 024103 DOI: 10.1063/1.2213976.

(71) Maurice, R.; Bastardis, R.; Graaf, C. De; Suaud, N.; Mallah, T.; Guihéry, N. Universal theoretical approach to extract anisotropic spin Hamiltonians. *J. Chem. Theory Comput.* **2009**, *5* (11), 2977–2984 DOI: 10.1021/ct900326e.

(72) Atanasov, M.; Ganyushin, D.; Sivalingam, K.; Neese, F. A modern first-principles view on ligand field theory through the eyes of correlated multireference wavefunctions. In *Molecular electronic structures of transition metal complexes II*; Mingos, D. M. P., Day, P., Dahl, J. P., Eds.; Structure and Bonding; Springer Berlin Heidelberg: Berlin, Heidelberg, 2012; Vol. 143, pp 149–220.

(73) Singh, S. K.; Eng, J.; Atanasov, M.; Neese, F. Covalency and chemical bonding in transition metal complexes: an ab initio based ligand field perspective. *Coord. Chem. Rev.* **2017**, *344*, 2–25 DOI: 10.1016/J.CCR.2017.03.018.

(74) Atanasov, M.; Daul, C. A. A.; Rauzy, C. New insights into the effects of covalency on the ligand field parameters: a DFT study. *Chem. Phys. Lett.* **2003**, *367* (5–6), 737–746 DOI: 10.1016/S0009-2614(02)01762-1.

(75) Atanasov, M.; Daul, C. A.; Rauzy, C. A DFT based ligand field theory. In *Optical spectra and chemical bonding in inorganic compounds*; Mingos, D. M. P., Schönherr, T., Eds.; Structure and Bonding; Springer Berlin Heidelberg: Berlin, Heidelberg, 2004; Vol. 106, pp 97–125.

(76) Baerends, E. J.; Autschbach, J.; Bashford, D.; Bérces, A.; Bickelhaupt, F. M.; Bo, C.; Boerrigter, P. M.; Cavallo, L.; Chong, D. P.; Deng, L.; et al. ADF program package version 2017.01. SCM, Amsterdam, The Netherlands.

(77) te Velde, G.; Bickelhaupt, F. M.; van Gisbergen, S. J. A.; Guerra, C. F.; Baerends, E. J.;

Snijders, J. G.; Ziegler, T.; Fonseca Guerra, C.; van Gisbergen, S. J. A.; Snijders, J. G.; et al. Chemistry with ADF. *J. Comput. Chem.* **2001**, *22* (9), 931–967 DOI: 10.1002/jcc.1056.

(78) Guerra, C. F.; Snijders, J. G.; te Velde, G.; Baerends, E. J. Towards an order-N DFT method. *Theor. Chem. Acc.* **1998**, *99*, 391–403.

(79) Swart, M.; Ehlers, A. W.; Lammertsma, K. Performance of the OPBE exchange-correlation functional. *Mol. Phys.* **2004**, *102* (23–24), 2467–2474 DOI: 10.1080/00268970420002750 17.

(80) Lenthe, E. van; Baerends, E. J.; Snijders, J. G. Relativistic regular two-component Hamiltonians. *J. Chem. Phys.* **1993**, *99* (6), 4597–4610 DOI: 10.1063/1.466059.

(81) van Lenthe, E.; Baerends, E. J.; Snijders, J. G. Relativistic total energy using regular approximations. *J. Chem. Phys.* **1994**, *101* (11), 9783–9792 DOI: 10.1063/1.467943.

(82) Becke, A. D. Density-functional thermochemistry. III. The role of exact exchange. *J. Chem. Phys.* **1993**, *98* (7), 5648–5652 DOI: 10.1063/1.464913.

(83) Carlin, R. L. *Magnetochemistry*; Springer Berlin Heidelberg: Berlin, Heidelberg, 1986.

(84) Krzystek, J.; Telser, J. Measuring giant anisotropy in paramagnetic transition metal complexes with relevance to single-ion magnetism. *Dalt. Trans.* **2016**, *45* (42), 16751–16763 DOI: 10.1039/C6DT01754A.

(85) Palion-Gazda, J.; Machura, B.; Kruszynski, R.; Grancha, T.; Moliner, N.; Lloret, F.; Julve, M. Spin Crossover in Double Salts Containing Six- and Four-Coordinate Cobalt(II) Ions. *Inorg. Chem.* **2017**, *56* (11), 6281–6296 DOI: 10.1021/acs.inorgchem.7b00360.

(86) Nemec, I.; Herchel, R.; Šilha, T.; Trávníček, Z. Towards a better understanding of magnetic exchange mediated by hydrogen bonds in Mn(iii)/Fe(iii) salen-type supramolecular dimers. *Dalt. Trans.* **2014**, *43* (41), 15602–15616 DOI: 10.1039/c4dt02025a.

(87) Blume, M.; Tjon, J. A. Mössbauer spectra in a fluctuating environment. *Phys. Rev.* **1968**, *165* (2), 446–456 DOI: 10.1103/PhysRev.165.446.

(88) Daul, C.; Zlatar, M.; Gruden-Pavlović, M.; Swart, M. Application of density functional and density functional based ligand field theory to spin states. In *Spin states in biochemistry and inorganic chemistry: influence on structure and reactivity*; Costas, M., Swart, M., Eds.; John Wiley & Sons, Ltd: Oxford, UK, 2015; pp 7–34.

(89) Vlahović, F.; Perić, M.; Gruden-Pavlović, M.; Zlatar, M. Assessment of TD-DFT and LF-DFT for study of d - d transitions in first row transition metal hexaaqua complexes. *J. Chem. Phys.* **2015**, *142* (21), 214111 DOI: 10.1063/1.4922111.

(90) Atanasov, M.; Jan Baerends, E.; Baettig, P.; Bruyndonckx, R.; Daul, C.; Rauzy, C.; Zbiri, M. The calculation of ESR parameters by density functional theory: the g- and A-tensors of Co(acacen). *Chem. Phys. Lett.* **2004**, *399* (4–6), 433–439 DOI: 10.1016/j.cplett.2004.10.041.

(91) Senn, F.; Zlatar, M.; Gruden-Pavlovic, M.; Daul, C. Computational analysis of tris(1,2-ethanediamine) cobalt(III) complex ion: calculation of the 59Co shielding tensor using LF-DFT. *Monatshefte für Chemie - Chem. Mon.* **2011**, *142* (6), 593–597 DOI: 10.1007/s00706-011-0491-9.

(92) Atanasov, M.; Daul, C. A. A DFT based ligand field model for magnetic exchange coupling in transition metal dimmer complexes: (i) principles. *Chem. Phys. Lett.* **2003**,

379 (3–4), 209–215 DOI: 10.1016/S0009-2614(03)01325-3.

(93) Matović, Z. D.; Jeremić, M. S.; Jelić, R. M.; Zlatar, M.; Jakovljević, I. Ž. Configurational, LFDFT and NBO analysis of chromium(III) complexes of edta-type ligands. *Polyhedron* **2013**, *55*, 131–143 DOI: 10.1016/j.poly.2013.02.079.

(94) Ramanantoanina, H.; Urland, W.; Cimpoesu, F.; Daul, C. Ligand field density functional theory calculation of the 4f2→ 4f15d1 transitions in the quantum cutter Cs2KYF6:Pr3+. *Phys. Chem. Chem. Phys.* **2013**, *15* (33), 13902–13910 DOI: 10.1039/c3cp51344k.

(95) Zlatar, M.; Gruden, M.; Vassilyeva, O. Y.; Buvaylo, E. A.; Ponomarev, A. N.; Zvyagin, S. A.; Wosnitza, J.; Krzystek, J.; Garcia-Fernandez, P.; Duboc, C. Origin of the zero-field splitting in mononuclear octahedral MnIV complexes: a combined experimental and theoretical investigation. *Inorg. Chem.* **2016**, *55* (3), 1192–1201 DOI: 10.1021/acs.inorgchem.5b02368.

(96) Garcia-Fernandez, P.; Senn, F.; Daul, C. A.; Aramburu, J. A.; Barriuso, M. T.; Moreno, M. The giant magnetic anisotropy energy of Fe+ ions in SrCl2. *Phys. Chem. Chem. Phys.* **2009**, *11* (35), 7545 DOI: 10.1039/b908110k.

(97) Wang, L.; Zlatar, M.; Vlahović, F.; Demeshko, S.; Philouze, C.; Molton, F.; Gennari, M.; Meyer, F.; Duboc, C.; Gruden, M. Experimental and theoretical identification of the origin of magnetic anisotropy in intermediate spin iron(III) complexes. *Chem. - A Eur. J.* **2018**, *24* (46), 11973–11982 DOI: 10.1002/chem.201705989.

(98) Singh, M. K.; Rajaraman, G. Can CH···π interactions be used to design single-chain magnets? *Chem. - A Eur. J.* **2015**, *21* (3), 980–983 DOI: 10.1002/chem.201404853.

(99) Pinsky, M.; Avnir, D. Continuous symmetry measures. 5. The classical polyhedra. **1998**, *37* (21), 5575–5582 DOI: 10.1021/IC9804925.

(100) Alvarez, S.; Alemany, P.; Casanova, D.; Cirera, J.; Llunell, M.; Avnir, D. Shape maps and polyhedral interconversion paths in transition metal chemistry. *Coord. Chem. Rev.* **2005**, *249* (17–18), 1693–1708 DOI: 10.1016/J.CCR.2005.03.031.

(101) Bersuker, I. B. *The Jahn-Teller effect*; Cambridge University Press, 2006.

(102) Zlatar, M.; Gruden, M. Calculation of the Jahn-Teller parameters with DFT. *J. Serb. Chem. Soc.* **2019**, *84* (8), 779–800 DOI: 10.2298/JSC190510064Z.

For Table of Contents (TOC) only:

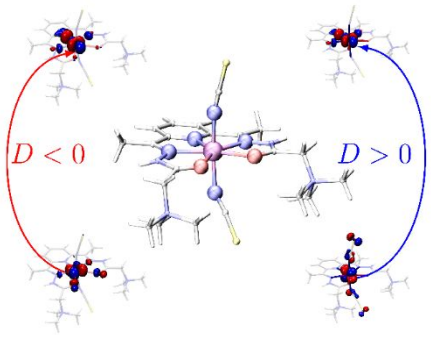

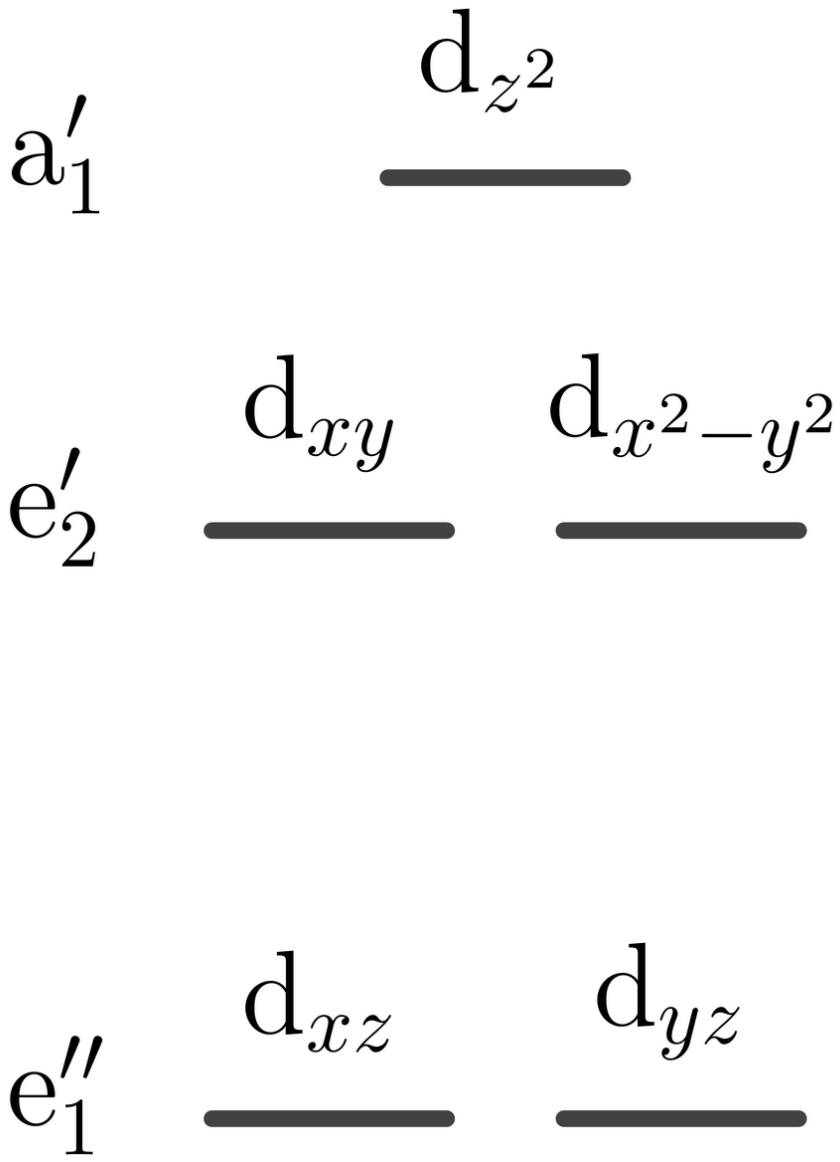

Figure 1a - Qualitative orbital splitting diagram for pentagonal bipyramidal (PBPY-7) coordination

38x51mm (600 x 600 DPI)

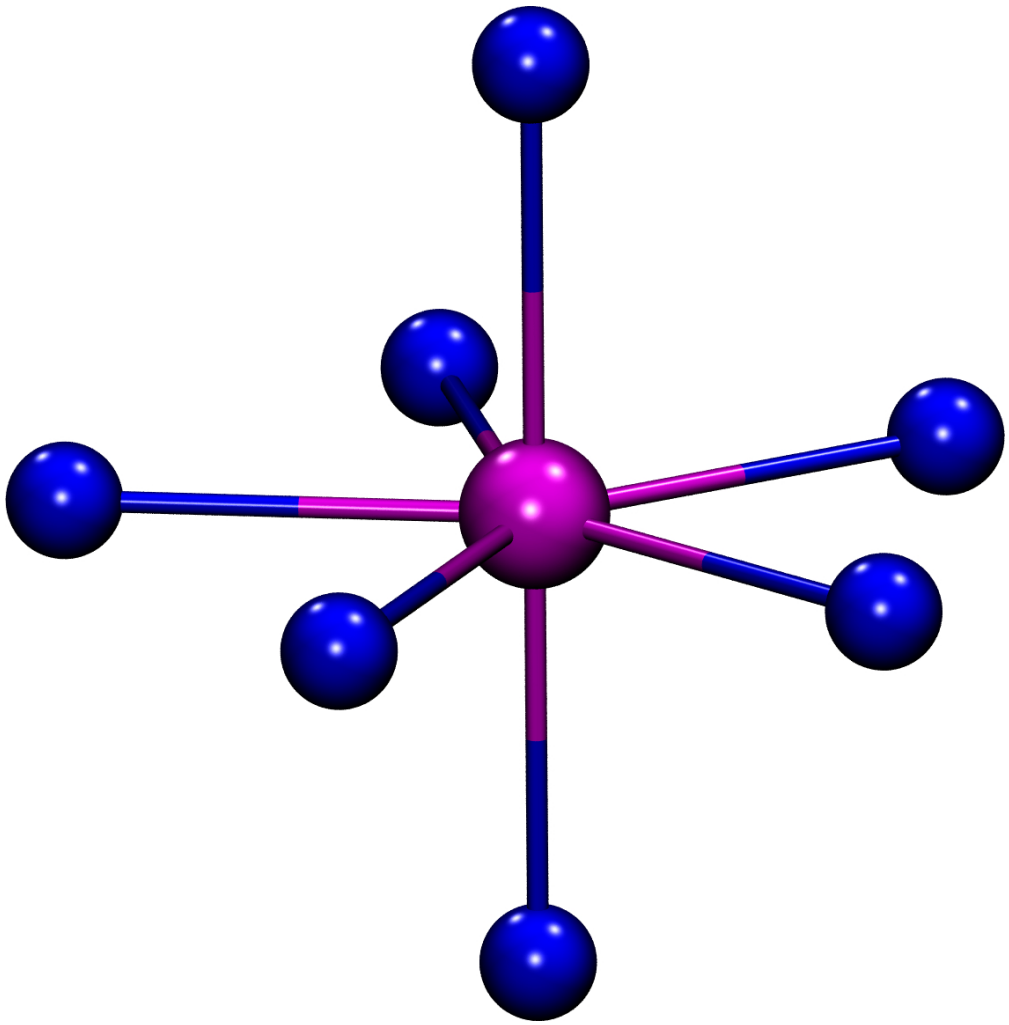

Figure 1b - PBPY-7 coordination

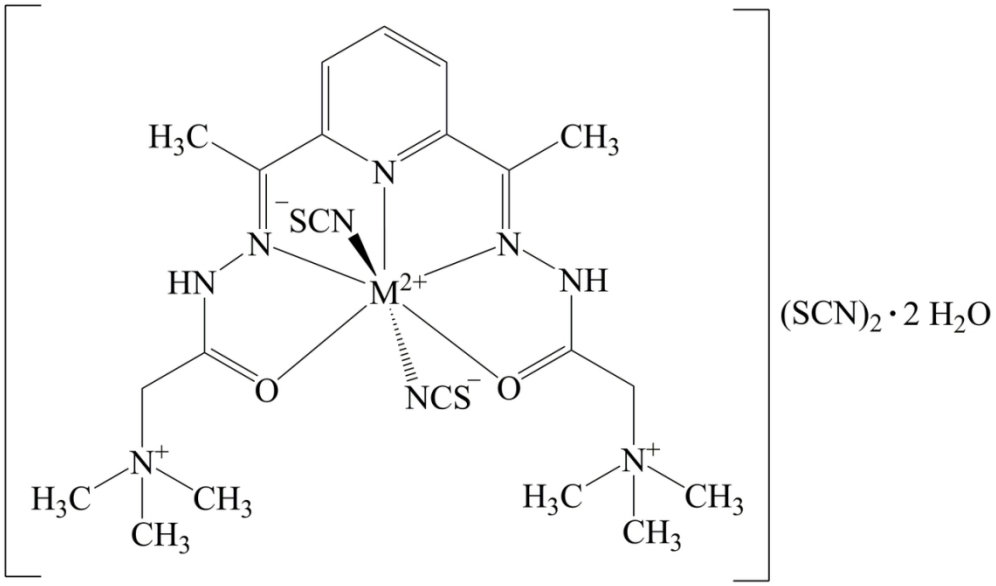

$[Co(\mathbf{H_2L})(NCS)_2](SCN)_2 \cdot 2H_2O$ (**1**) (M=Co)

$[Ni(\mathbf{H_2L})(NCS)_2](SCN)_2 \cdot 2H_2O$ (**5**) (M=Ni)

Scheme 1a - Structures of pentagonal-bipyramidal complexes 1 and 5

111x81mm (300 x 300 DPI)

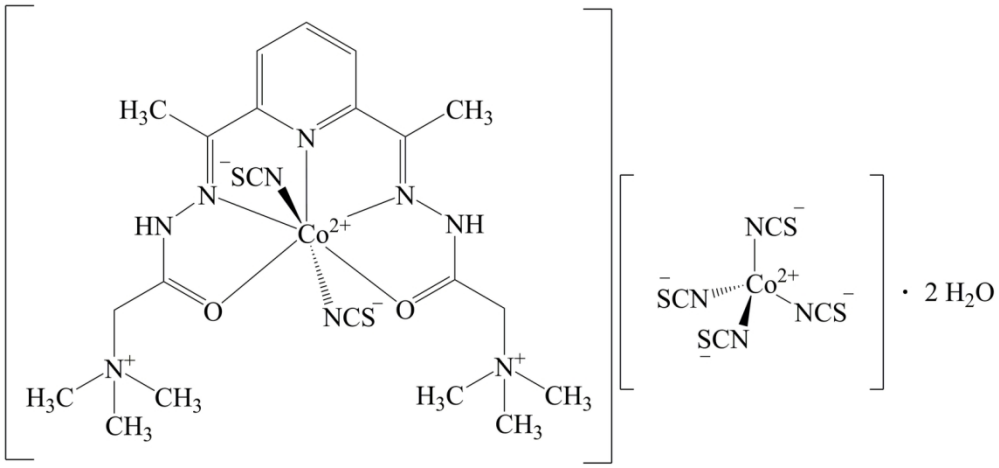

$[Co(\mathbf{H_2L})(NCS)_2][Co(NCS)_4]\cdot 2H_2O$ **(2)**

Scheme 1b - Structures of pentagonal-bipyramidal complex 2

140x74mm (300 x 300 DPI)

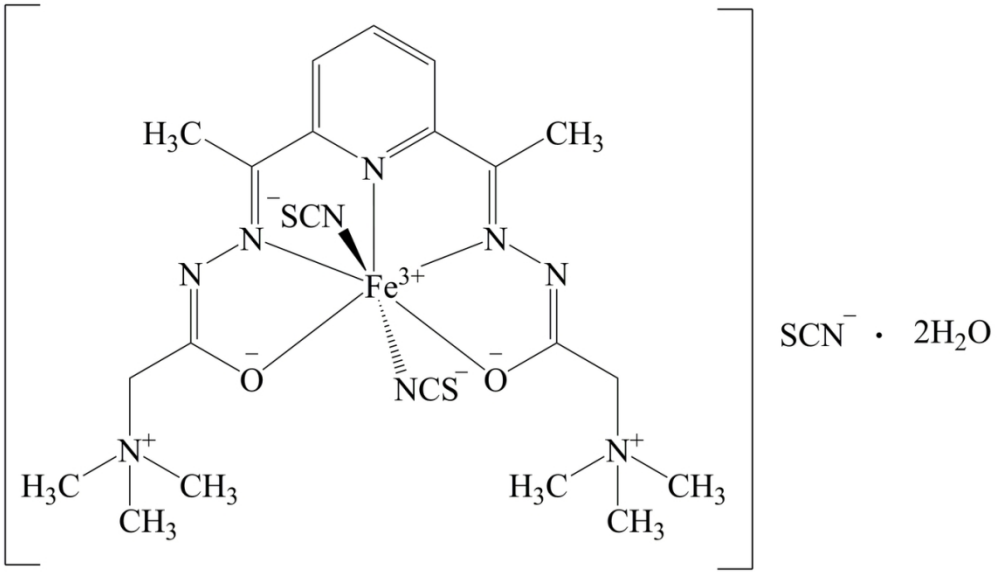

$[Fe(\mathbf{L})(NCS)_2](SCN)\cdot 2H_2O$ (**3**)

Scheme 1c - Structures of pentagonal-bipyramidal complex 3

114x82mm (300 x 300 DPI)

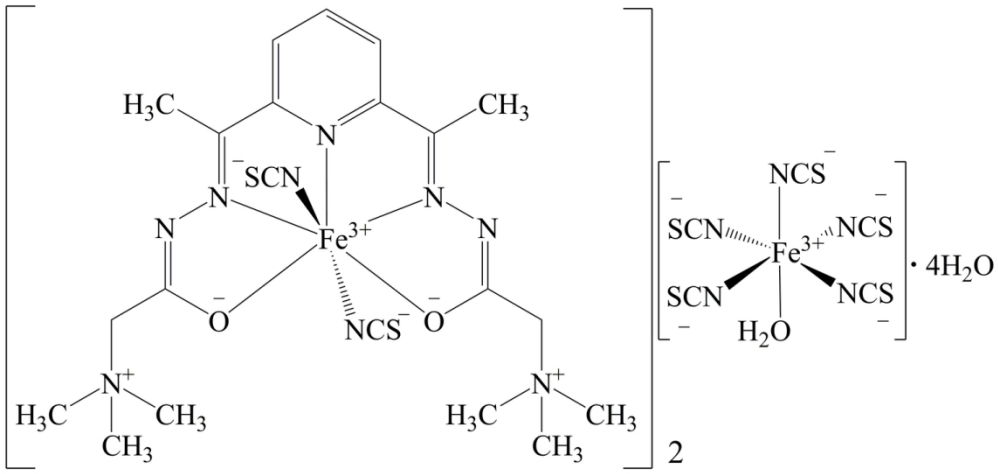

$[Fe(\mathbf{L})(NCS)_2][Fe(NCS)_5(H_2O)]\cdot 4H_2O$ (**4**)

Scheme 1d - Structures of pentagonal-bipyramidal complex 4

129x77mm (300 x 300 DPI)

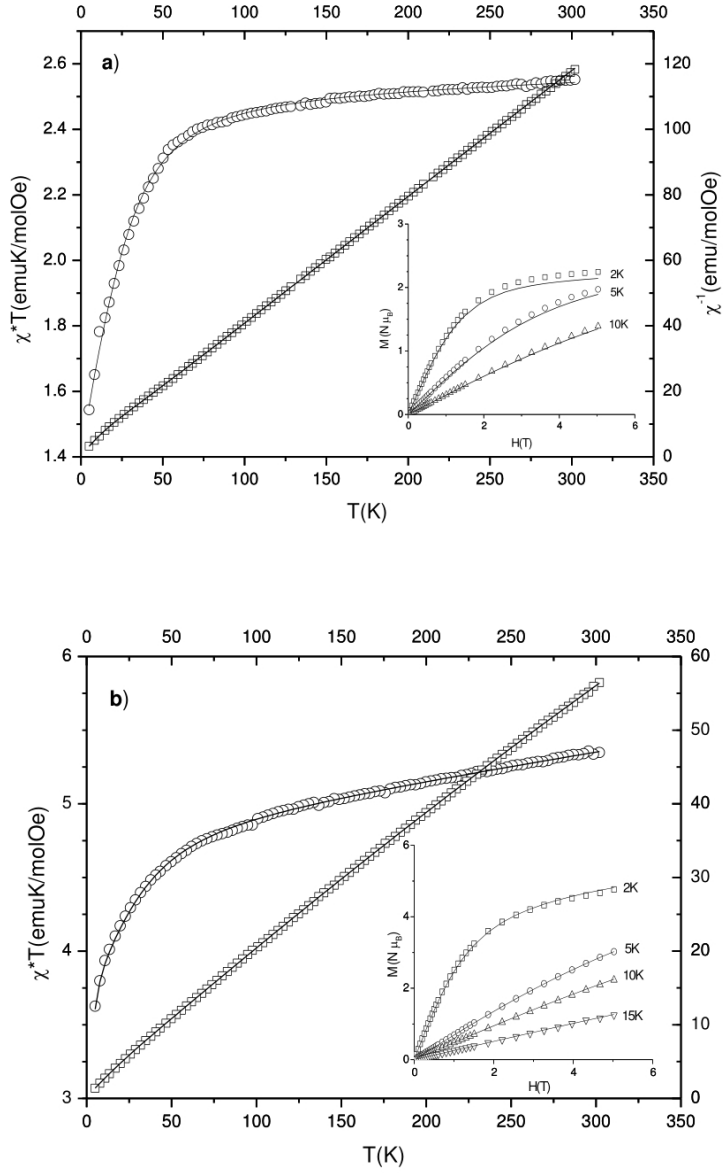

Fig. 2 Magnetic measurements for 1 and 2

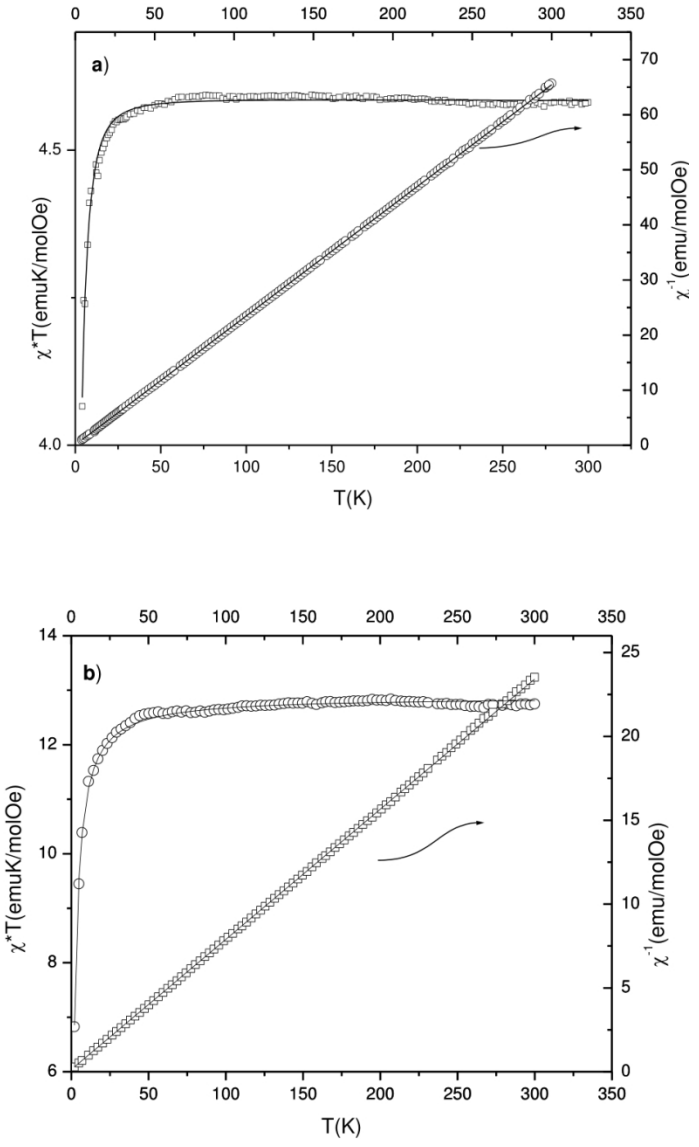

Fig. 3 Magnetic measurements for 3 and 4

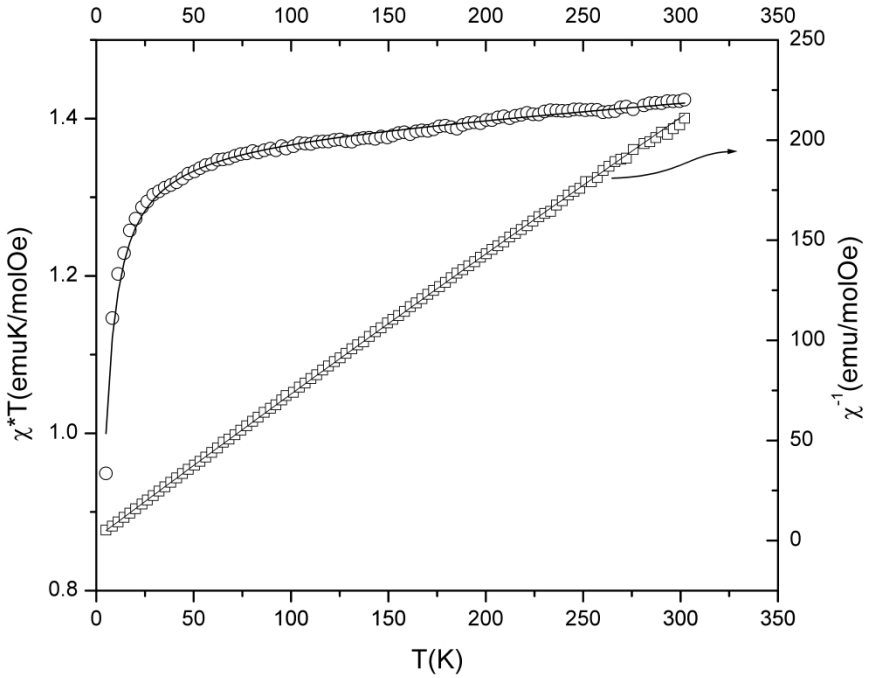

Figure 4 - Magnetic measurements for 5

1083x829mm (150 x 150 DPI)

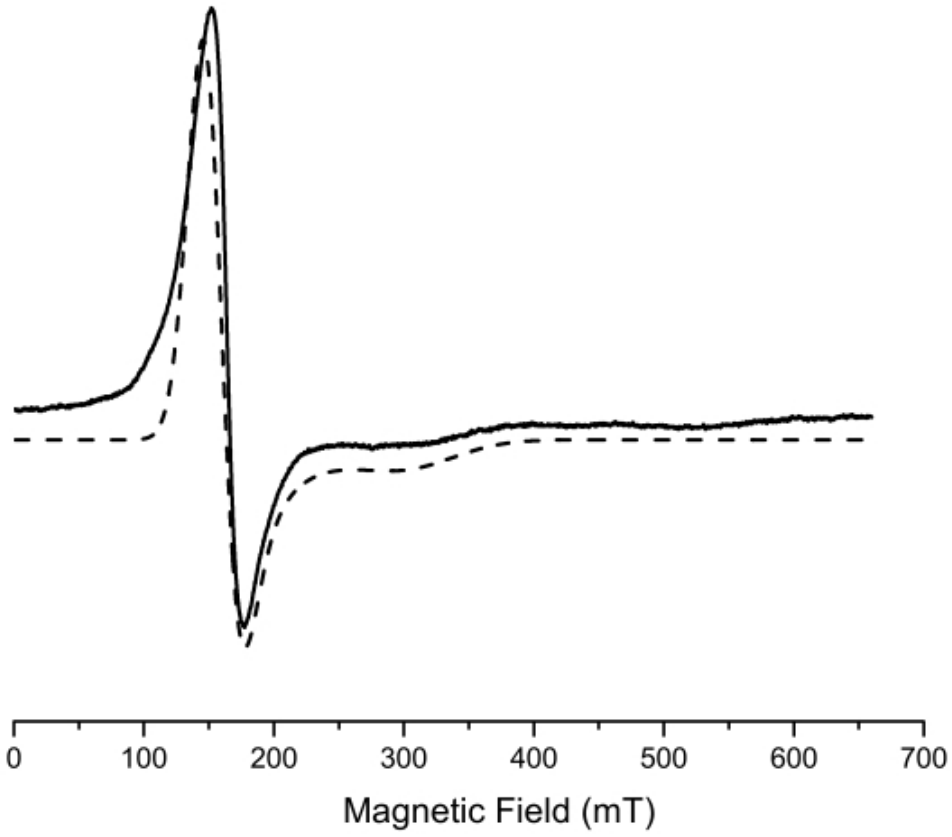

Figure 5a - EPR for 1

93x81mm (150 x 150 DPI)

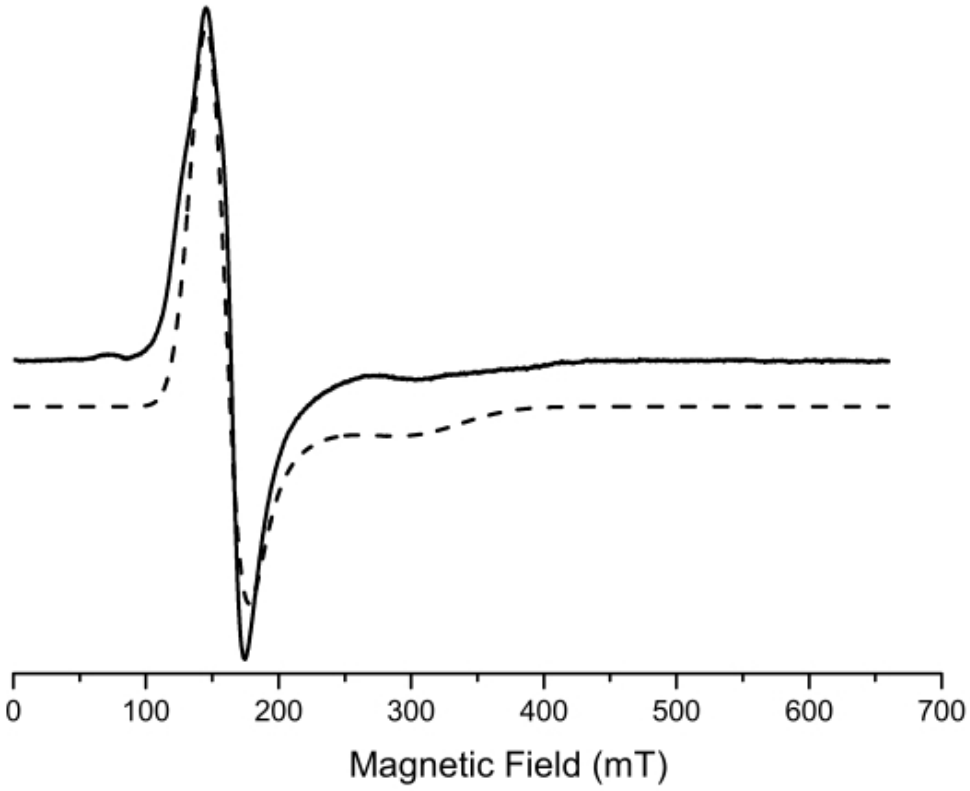

Figure 5b - EPR for 2

91x81mm (150 x 150 DPI)

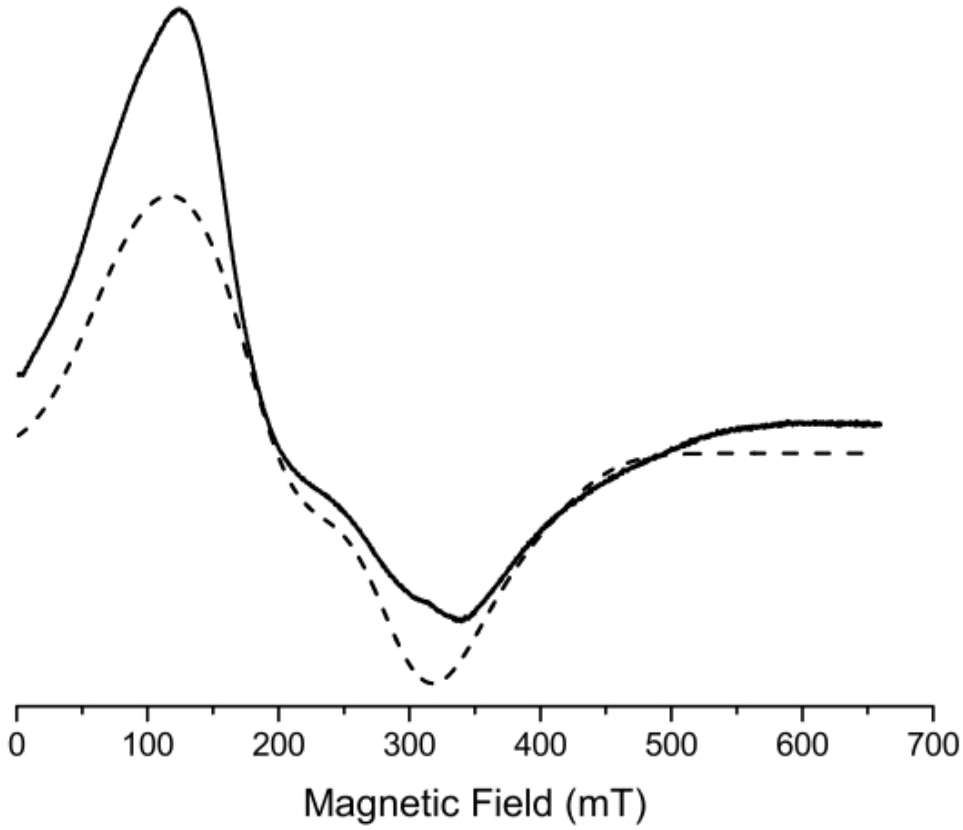

Figure 6a - EPR for 3

93x81mm (150 x 150 DPI)

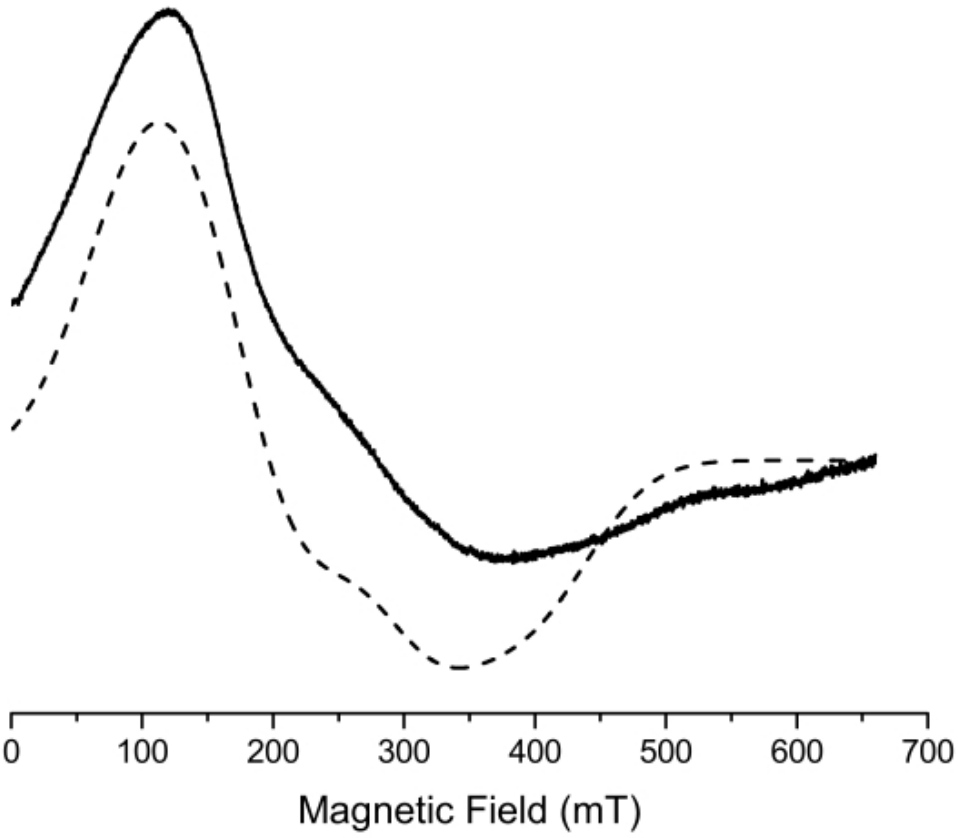

Figure 6b - EPR for 4

93x83mm (150 x 150 DPI)

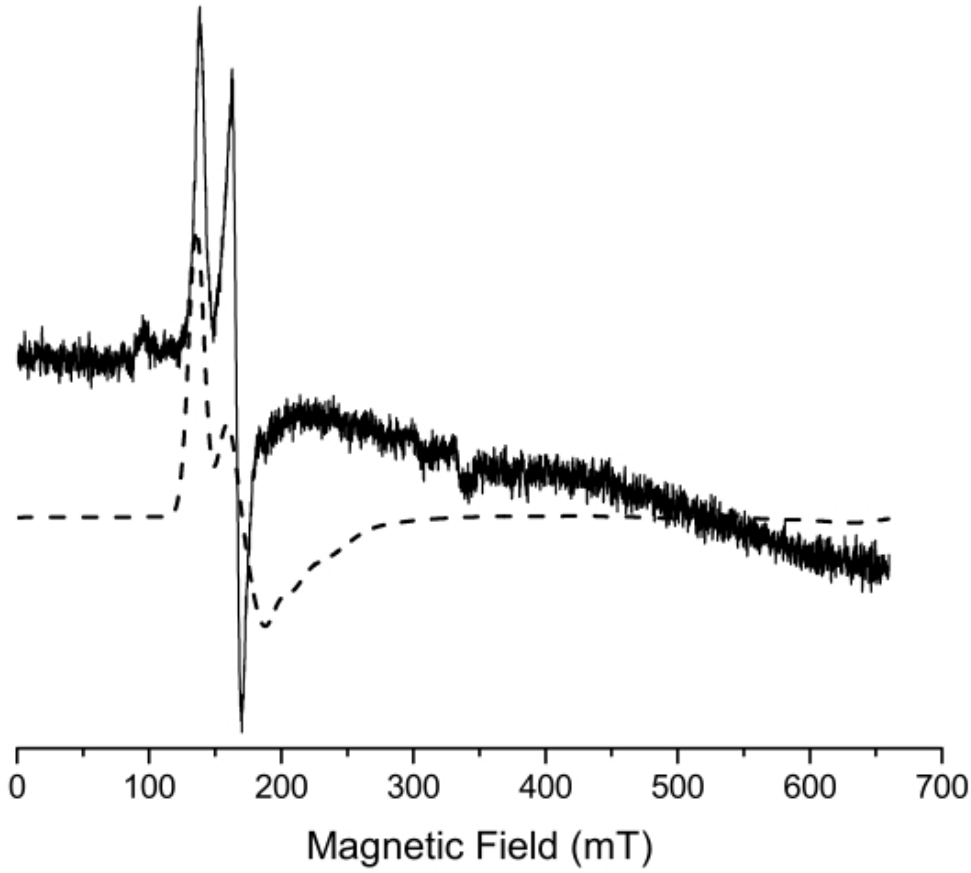

Figure 7 - EPR for 5

92x84mm (150 x 150 DPI)

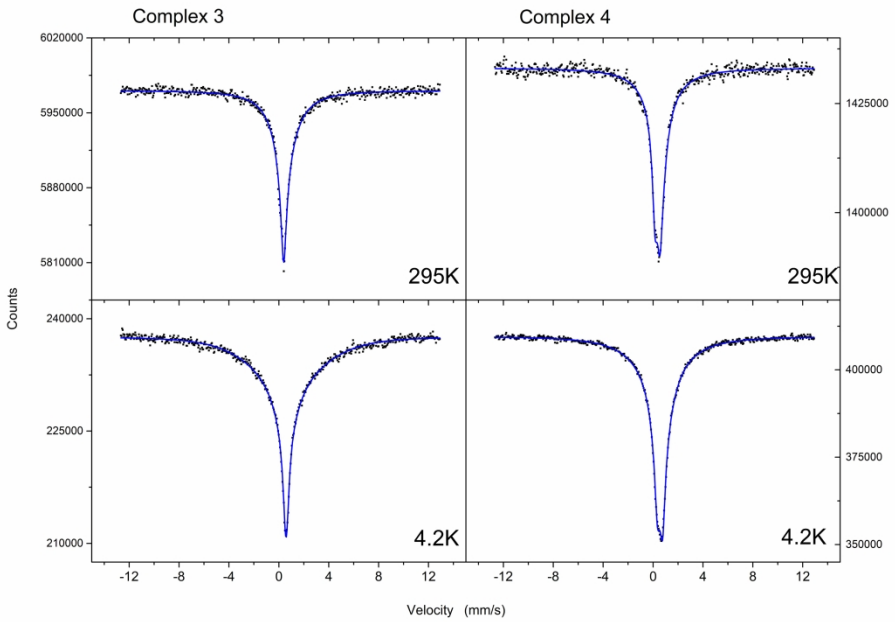

Figure 8 - 57Fe Mössbauer spectra of complexes 3 and 4 recorded at 295K and

144x101mm (600 x 600 DPI)

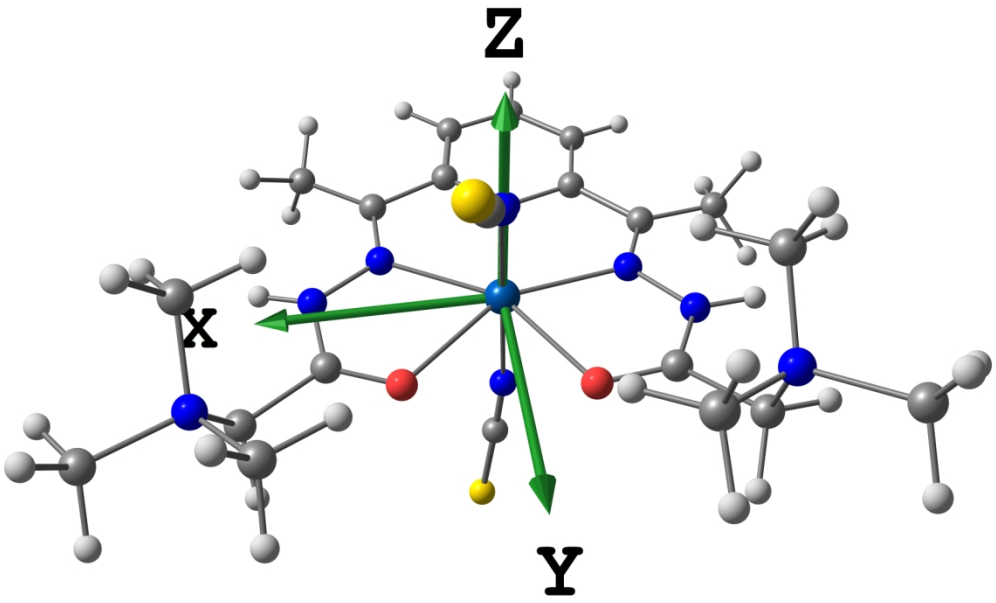

Figure 9a - Orientation of the molecule 1 in D-tensor frame

465x278mm (96 x 96 DPI)

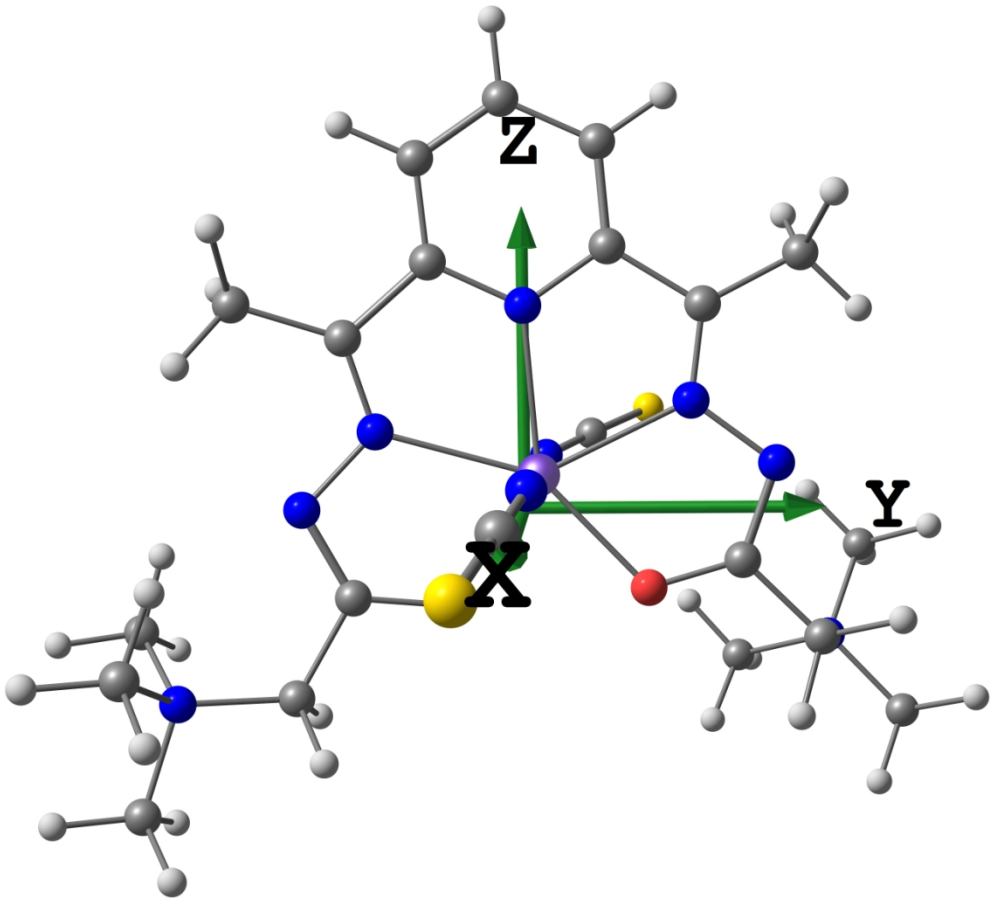

Figure 9b - Orientation of the molecule 3 in D-tensor frame

347x314mm (96 x 96 DPI)

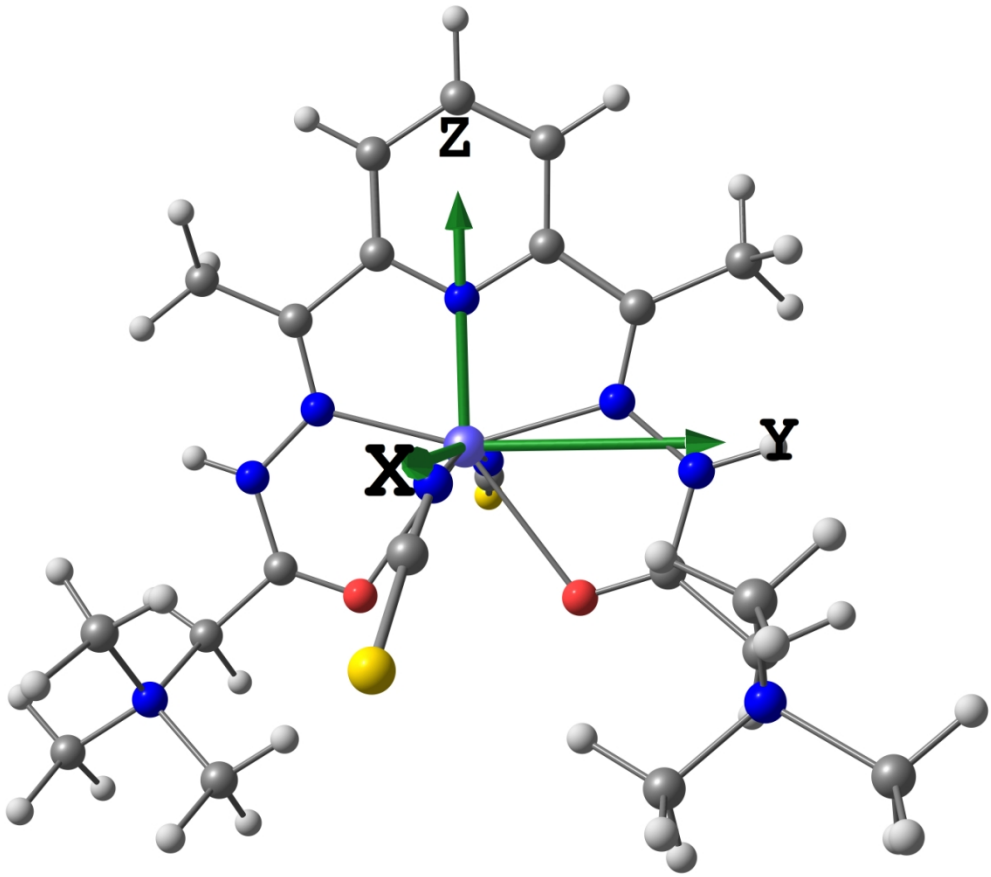

Figure 9c - Orientation of the molecule 5 in D-tensor frame

355x314mm (96 x 96 DPI)

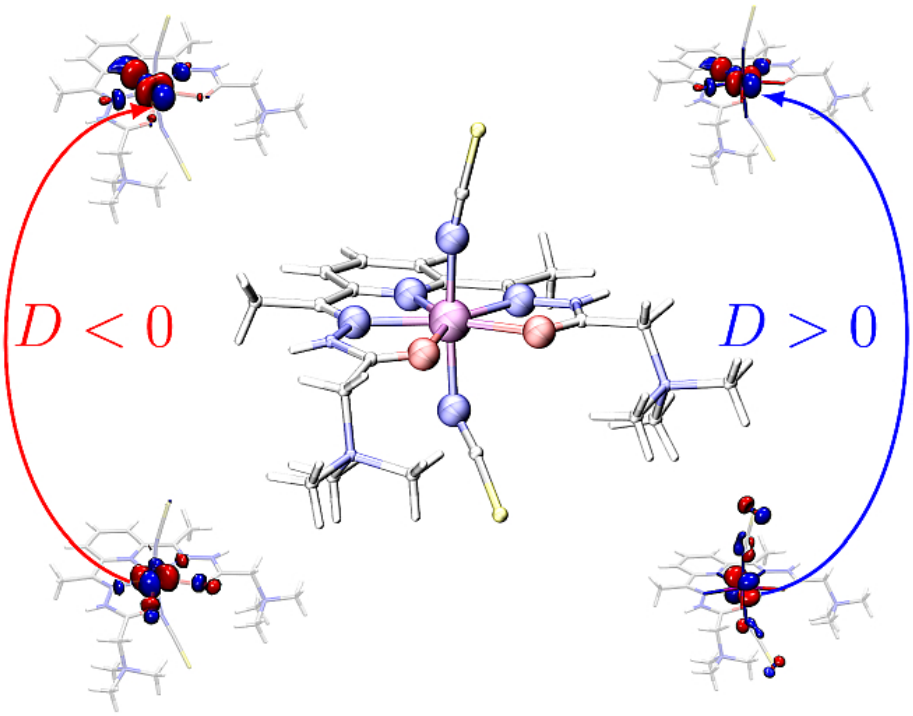

60x44mm (300 x 300 DPI)